A polynomial chaos framework for probabilistic predictions of storm surge events

Pierre Sochala[1] · Chen Chen[2] · Clint Dawson[2] · Mohamed Iskandarani[3]

Abstract

We present a polynomial chaos-based framework to quantify the uncertainties in predicting hurricane-induced storm surges. Perturbation strategies are proposed to characterize poorly known time-dependent input parameters, such as tropical cyclone track and wind as well as space-dependent bottom stresses, using a handful of stochastic variables. The input uncertainties are then propagated through an ensemble calculation and a model surrogate is constructed to represent the changes in model output caused by changes in the model input. The statistical analysis is then performed using the model surrogate once its reliability has been established. The procedure is illustrated by simulating the flooding caused by Hurricane Gustav 2008 using the ADvanced CIRCulation model. The hurricane's track and intensity are perturbed along with the bottom friction coefficients. A sensitivity analysis suggests that the track of the tropical cyclone is the dominant contributor to the peak water level forecast, while uncertainties in wind speed and in the bottom friction coefficient show minor contributions. Exceedance probability maps with different levels are also estimated to identify the most vulnerable areas.

Keywords Tropical cyclones · Uncertainty quantification · Empirical orthogonal functions · Global sensitivity analysis · Exceedance probability · Hurricane Gustav

1 Introduction

Hurricanes are unanimously recognized as severe threats to coastal communities due to their high winds, and the associated risks they bring such as tornadoes, and floodings from intense rain and storm surges. Storm surges constitute, in particular, the greatest hazards to life and property and their devastating impact has been documented during hurricanes Katrina and Wilma in 2005, Ike in 2008, Sandy in 2012, and Harvey and Irma in 2017 (https://www.nhc.noaa.gov/surge/ contains a list of damages). Storm surge models in these circumstances can be extremely useful tools in warning coastal communities about the risks of a

particular storm surge event, in mitigating the loss of lives and properties, and in assisting in coastal risk management and prevention.

The aim of this article is to present a framework for probabilistic storm surge prediction that produces, in addition to the most likely forecast, an estimate of the uncertainties in that forecast. The probabilistic framework accounts for the uncertainties in various poorly known quantities including storm characteristics (track and intensity) and empirical constitutive laws (wind drag and bottom friction). Our approach is based on a surrogate (a.k.a meta-model, emulator, response surface, or proxy) that can explicitly provide the changes in the storm surge model's output, e.g. the peak water level elevation, caused by changes in the model's uncertain inputs. This surrogate can be built using either Gaussian process regression or, as was done here, orthogonal polynomials series (the polynomial chaos). The main advantages of a surrogate are (i) to efficiently propagate the uncertainties in the model inputs in order to compute the uncertainties in the model output, (ii) to identify the dominant contributors to the output uncertainties through the sensitivity analysis, and (iii) to perform parameter calibrations efficiently (the so-called backward propagation) if observational data is available. From a practical point of view, the

✉ Pierre Sochala
  p.sochala@brgm.fr

[1] BRGM, 3 Avenue Claude Guillemin, 45060, Orléans, France

[2] Oden Institute for Computational Engineering and Sciences, University of Texas at Austin, Austin, TX 78712, USA

[3] Rosenstiel School of Marine and Atmospheric Science, University of Miami, Miami, FL 33149, USA

surrogate is built unintrusively (i.e., without changes to the storm surge model that is treated as a "black box") at the cost of performing ensemble calculations. The input-output relationships of the ensemble members are in fact exploited to obtain a simplified representation of the model output whose computational cost is negligible in comparison with storm surge model evaluation. Polynomial chaos expansions have recently been used to quantify uncertainties in various geoscience disciplines such as oceanic and atmospheric flows [11, 23, 28, 29], subsurface flows [26, 45], seismic wave propagation [44], and geochemical compaction [14]. Polynomial chaos surrogates are also extremely useful in enabling and accelerating Bayesian inference as was done for subsurface flows [10], debris flows [38], and earthquake parameters calibration [7, 16].

Although many processes contribute to changes in coastal water levels during a hurricane landfall (such as tides, wave breaking, fresh water inputs from rivers and rainfall, and atmospheric pressure) the focus here is on the dominant storm surge generated by hurricane winds pushing waters onshore. The dynamics are adequately described by the barotropic shallow water equations with prescribed forcing at the ocean surface and along the offshore lateral boundaries of the domain. We thus adopt the barotropic version of advanced circulation (ADCIRC) model, with its unstructured finite element grid and its wetting and drying capabilities, as the storm surge model. The model's uncertain inputs can be classified under two broad categories: those associated with the atmospheric forcing and those associated with the ocean model parameterizations. Two instances of the latter category include the parameterization of the surface wind stresses via a wind drag law and of the bottom stresses via a friction law.

The proposed approach is illustrated to simulate the storm surge stemming from Hurricane Gustav 2008. Specifically, the uncertain sources considered are the hurricane track and winds and the bottom friction coefficients in marshland and forested areas. Ideally, the wind input would be specified from a meteorological forecast that accounts explicitly for the complex multiphysics and multiscale dynamics of a hurricane. Here, and in the spirit of a proof of concept illustration, we take a simpler approach with the idealized hurricane wind profile proposed by Holland in [19] and using the best track (BT) data as reference. Ensemble simulations are then performed to propagate the uncertainties in the model input in order to estimate the uncertainties and the statistical information on the storm surge output. The probability of threshold overrun is evaluated to locate the most vulnerable areas. We conduct a sensitivity analysis to identify which of the uncertain inputs is the dominant contributor to the uncertainty of the maximum water elevation. Our finding is that the hurricane trajectory is the main contributor while the intensity and the bottom friction terms play a secondary role.

The procedure outlined above can be applied to other hurricanes as well. The following steps must be carried out for a particular event: (i) the identification of the relevant uncertain input data for that event (Section 4 provides a fairly general template particularly for the atmospheric forcing), (ii) the sampling of the ensuing uncertain input parameter space, and the computations of the corresponding model outputs using the actual storm surge numerical code (here ADCIRC), (iii) the surrogate construction and validation by using the results of ensemble simulations (see Section 5), and (iv) the statistical analysis using the surrogate (see Section 6).

The present framework should not be confused with other approaches used to deal with uncertainties arising in oceanic and meteorological forecasts especially in storm surges prediction. For long time scales (several decades, century), the threat of storm events can be measured by their return periods. The joint-probability method (JPM) [37] has been developed for the purpose of estimating extreme hurricane surge frequencies in [22, 46, 48, 50]. For short time scale (few days, one week), the ensemble prediction system (EPS) technique perturbs the initial condition of the system in order to produce different (realistic) forecasting realizations. The EPS technique has been applied in particular for surge forecasting in [12, 34, 35]. The focus of this article is also on forecasting a specific, near-future event but with uncertainty sources not only on the initial condition, as done for the example in [42] and in [24] for synthetic storms. Previous investigations of storm surge uncertainties have focused on different aspects of the surge's impact which include flooding of urban areas [4], dependency between extreme rainfall and the surge [51], and site-specific estimates of damage [41].

The outline of this paper is as follows. Section 2 presents the physical model setup and the case study description. Section 3 describes the uncertainty setting including the probabilistic framework and the steps needed to quantify uncertainties in simulations. Section 4 details the perturbation of the uncertain time-dependent parameters (track and maximum wind speed) and the friction coefficient. The construction of the space-dependent peak water level surrogate is described in Section 5. In Section 6, after a description of our two test scenarios, the results focus on the surrogate validation, the sensitivity fields and the exceedance probability maps for each scenario. Conclusions and perspectives are drawn in Section 7.

2 Physical model

This section presents briefly the storm surge forecast model, the identification and characterization of its uncertain inputs, the meteorological forcing model, and a description of Hurricane Gustav 2008.

2.1 Storm surge model

The barotropic version of the ADCIRC model [32] is adopted herein to simulate storm surges. ADCIRC has been extensively tested and validated, and is used by a broad community to simulate a wide range of oceanic, coastal, and estuarine flows, including hurricane-induced storm surges such as those caused by hurricanes Katrina and Rita [8], Ike [25], and Gustav [9, 13, 17]. The system of equations solved by ADCIRC consists of the continuity and the momentum equations whose unknows are the 2D depth-averaged velocity field $\boldsymbol{v} = (v_x, v_y)^\top$ and the total water column height h (defined as the water depth plus the bathymetric depth),

$$\partial_t h + \nabla \cdot (h\boldsymbol{v}) = 0, \tag{1a}$$

$$\partial_t (h\boldsymbol{v}) + \nabla \cdot (h\boldsymbol{v} \otimes \boldsymbol{v}) + f h \boldsymbol{v}_r = -gh\nabla \tilde{p} + \cdots$$
$$\boldsymbol{S} + \frac{(\tau_s - \tau_b)}{\rho_w}, \tag{1b}$$

where f is the Coriolis parameter, $\boldsymbol{v}_r = (-v_y, v_x)^\top$, g the gravity, and ρ_w the water density. The term $\tilde{p}$ in Eq. 1b is the sum of the free surface elevation, the atmospheric pressure, and the tidal potential while the term $\boldsymbol{S}$ collects the vertically integrated lateral stress gradients, the momentum dispersion terms, and the vertically integrated baroclinic pressure gradients (see [32] for a complete derivation of system (1)). The nonlinear interactions of the astronomical tide and surge can play a significant role in coastal flooding as shown in [18]; their effects can be included easily in ADCIRC by adding the tidal potential to $\tilde{p}$. The tidal terms are omitted here for simplicity to focus on the uncertainties in the atmospheric forcing and the model's parameterization of bottom stresses.

The wind and bottom stresses τ_s and τ_b are major sources of input uncertainties as they depend on uncertain wind patterns and on parameterizations which, in turn, depends on empirical constants that are sometimes poorly constrained by observations. The details of these parameterizations are now presented.

2.2 Wind and bottom drag parameterizations

The surface stresses in the ADCIRC momentum (1b) is parameterized using the drag law [47],

$$\tau_s(\boldsymbol{v}_{10}) = \rho_a \, C_d(\boldsymbol{v}_{10}) \, |\boldsymbol{v}_{10}| \, \boldsymbol{v}_{10}, \tag{2}$$

where ρ_a refers to the air density, $\boldsymbol{v}_{10}$ to the 10 m wind vector (with $|\boldsymbol{v}_{10}|$ its speed), and $C_d(\boldsymbol{v}_{10})$ denotes the dimensionless and wind-dependent wind drag coefficient. ADCIRC relies on a three-sector based (left, right, and rear) wind drag coefficient [9, 40]. Uncertainties in $\boldsymbol{v}_{10}$ impact the wind stress calculations directly through the quadratic dependence of τ_s on the wind, and indirectly through their impacts on the drag coefficient.

The bottom stresses τ_b are defined using a quadratic law as well:

$$\tau_b(\boldsymbol{v}) = \rho_w C_f(\boldsymbol{x}) \, |\boldsymbol{v}| \, \boldsymbol{v}, \tag{3}$$

where C_f is the bottom friction coefficient and $\boldsymbol{x}$ the spatial coordinates. We use Manning's formula:

$$C_f(\boldsymbol{x}) = \frac{g \mathsf{n}(\boldsymbol{x})^2}{h^{1/3}}, \tag{4}$$

where $\mathsf{n}(\boldsymbol{x})$ is the spatially varying Manning roughness coefficient. For h sufficiently small, C_f is set to a constant to prevent division by zero [17]. The Manning coefficient impacts momentum loss caused by bottom stresses and its specification is hindered by a great deal of uncertainty (as caused, for example, by changes in vegetation) that we take into account in this study (see [17] for a discussion on the uncertainty sources on the Manning coefficient and [33] for calibration using Kalman filters).

2.3 Meteorological forcing model

Ideally, the atmospheric conditions needed to force the storm surge model would be obtained from a numerical forecast. Here, we resort to a parametric representation of the hurricane wind field which is commonly used when costly ensemble simulations must be performed. We thus adopt the Holland model to specify the tangential wind speed component (see Appendix); other parametric models can also be used [30]. The time-dependent quantities characterizing the Holland hurricane wind fields are the latitude $\varphi(t)$ and longitude $\lambda(t)$ of the minimum sea level pressure (that define the hurricane track), the maximum wind speed $v_{max}(t)$, the central pressure $p_c(t)$, and the maximum winds radius $R_{mw}(t)$.

2.4 Case study description

We propose to take into account the uncertainty in forecasting the storm surge caused by Hurricane Gustav, a major hurricane of the 2008 Atlantic season. Gustav formed on the 25 August with successive landfalls in Haïti, Jamaica, Cayman Islands, Cuba and made its final landfall on 1 September 15h00 UTC as a category 2 hurricane at Cocodrie in southern Louisiana. Hurricane Gustav has been
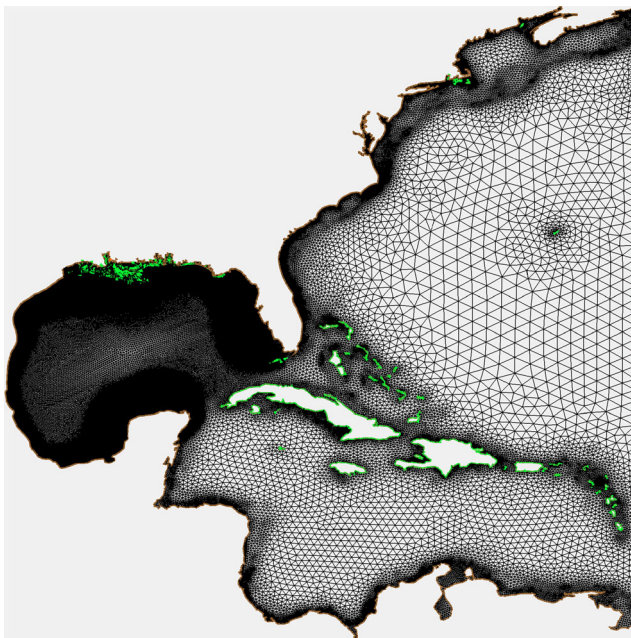
Fig. 1 Mesh of the computational domain

the subject of many studies. Forbes et al. [13] analyzed the storm surge variability by using twenty realizations and compared simulated and observed water level at coastal and inland stations. Dietrich et al. [9] used data-assimilated winds and several computational models to provide a synoptic analysis of the waves and water levels. More recently, Graham et al. [17] estimated the bottom friction coefficient in a coastal inlet with data obtained from a hindcast study of Gustav.
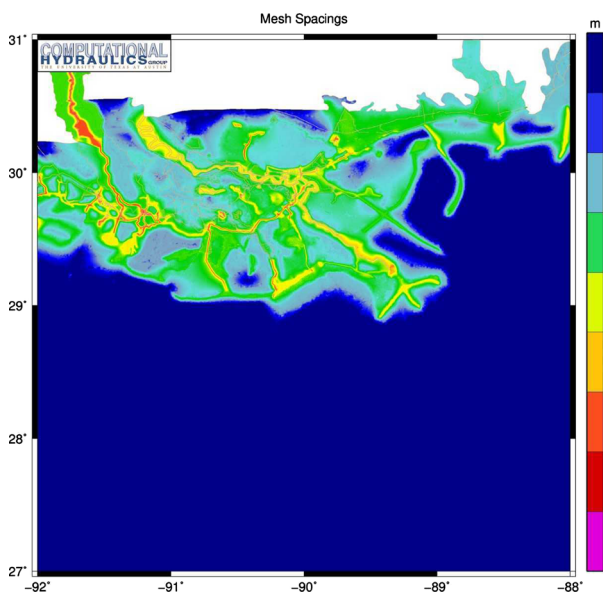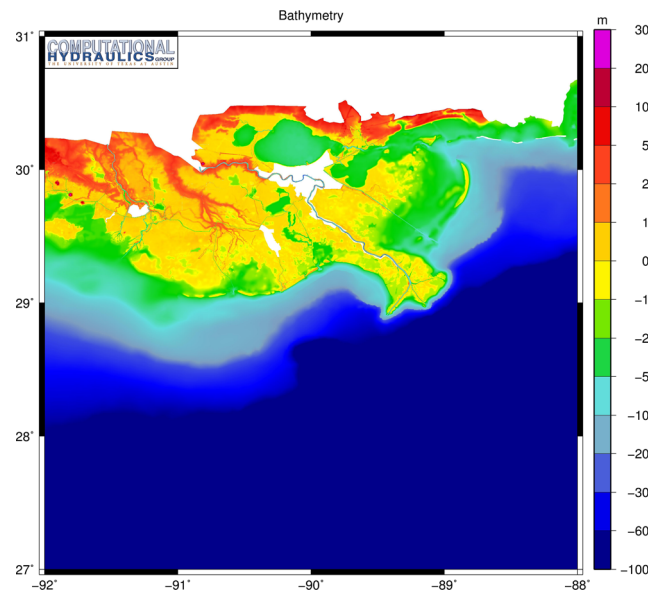

Fig. 3 Bathymetry/topography (m) in the Southeastern Louisiana

We are interested here in quantifying the uncertainty in forecasting the storm surge's peak water level (PWL) over the simulation time defined as

$$H(\boldsymbol{x}) = \max_t \left(h(\boldsymbol{x}, t) \right),$$

where t is the time variable. The computational domain covers the Gulf of Mexico, the Caribbean Sea, and the western North Atlantic Ocean as shown in Fig. 1. The mesh has 1,329,457 triangular elements and 678,915 nodes with a finer coastal resolution varying from 400 to 50 m as illustrated in Fig. 2, where the mesh resolution is plotted for Southeastern Louisiana. The bathymetry is shown in Fig. 3 and the unperturbed Manning coefficient is depicted
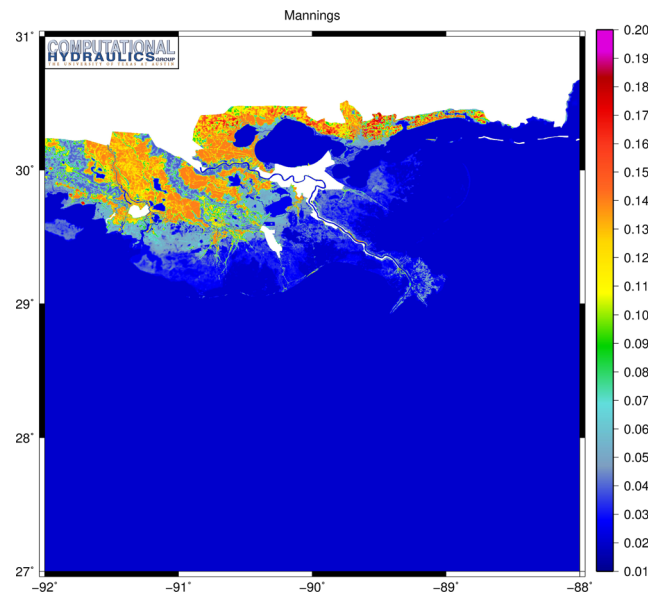

Fig. 2 Mesh resolution (m) in the Southeastern Louisiana

Fig. 4 Manning's values in the Southeastern Louisiana

in Fig. 4. The time step was set to 1 s and 302,400 time steps were needed to simulate 3.5 days. The computational time of each ADCIRC ensemble run is about 1 h 15 min using 120 CPUs.

3 Uncertainty quantification methodology

The present section introduces the essential ingredients and the probabilistic framework of uncertainty quantification, the motivation for adopting a surrogate approach, and the main tasks required to implement the proposed methodology.

3.1 Probabilistic framework

The storm surge forecast requires the specification of a substantial amount of input data, such as initial and boundary conditions, and, most importantly for the present application, the sources (surface wind stresses) and sinks (bottom drag) of momentum. These momentum sources and sinks involve empirical wind drag and friction coefficients along with a specification of the surface wind velocity. All these quantities are only known approximately, and their uncertainties impact the reliability of the storm surge forecast and justifies the use of a probabilistic approach. The quantification of this uncertainty requires the following steps:

1. The identification of the uncertain input data, along with their statistical distributions. For a scalar parameter θ, this is tantamount to specifying a range (or support) $[\theta_{\min}, \theta_{\max}]$ and a density function $p_\theta(\theta)$. It is common to introduce a canonical (standard) random variable ξ that maps θ linearly to the interval $[-1, 1] \ni \xi$. The process is repeated for all the independent uncertain parameters and the collection of stochastic variables are assembled into a random vector $\boldsymbol{\xi}$. Let $\varXi$ be the domain of $\boldsymbol{\xi}$ and $p_{\boldsymbol{\xi}}(\boldsymbol{\xi})$ its probability density function given by the product of the individual pdfs on account of their independence.
2. The stochastic domain $\varXi$ is sampled according to $p_{\boldsymbol{\xi}}(\boldsymbol{\xi})$ providing $\{\boldsymbol{\xi}^{(1)}, \cdots, \boldsymbol{\xi}^{(N)}\}$ the sample set of inputs. The corresponding direct ADCIRC simulations are then performed to produce the N model outputs $\{h^{(1)}(\boldsymbol{x}, t), \cdots, h^{(N)}(\boldsymbol{x}, t)\}$.
3. As a result, the PWL depends not only on the variable of space but also on the input data and we can write $H(\boldsymbol{x}, \boldsymbol{\xi})$. Our primary interest is in the statistical information of the PWL which includes the *first moments* (mean and variance):

$$\mathbb{E}(H) = \int H(\boldsymbol{x}, \boldsymbol{\xi}) p_{\boldsymbol{\xi}}(\boldsymbol{\xi}) \mathrm{d}\boldsymbol{\xi}, \tag{5}$$

$$\mathbb{V}(H) = \int (H(\boldsymbol{x}, \boldsymbol{\xi}) - \mathbb{E}(H))^2 \, p_{\boldsymbol{\xi}}(\boldsymbol{\xi}) \mathrm{d}\boldsymbol{\xi}, \tag{6}$$

the *sensitivity indices* (see Section 5.3) to identify the dominant contributors to the forecast uncertainty, and the *exceedance probabilities* (see Section 5.4).

3.2 Surrogate approach

A conventional method to compute the output uncertainties and their moments is via Monte Carlo sampling, whereby an ensemble of simulations is performed with randomly selected input data. The convergence rate of the Monte Carlo method is independent of the dimension of the uncertain space but is rather slow (the error in estimating the mean, for example, decreases as the square root of the number of realizations). As a consequence, the number of ensemble members needed to estimate the statistical moments with high accuracy increases dramatically with the dimension of the uncertain vector $\boldsymbol{\xi}$ and becomes nearly impractical when the storm surge model is computationally expensive and can only be run hundreds of times, as opposed to millions of times. In this paper, we adopt the surrogate (or meta-model) approach where an efficient and reliable approximation of the model is constructed using a small ensemble (see Section 5). This surrogate permits the user to approximate faithfully and efficiently the changes in a specific model output caused by changes in the model inputs; the surrogate can then be used in lieu of the model to perform the statistical analyses and explore the input parameter space.

3.3 Practical implementation

Algorithm 1 provides an overview of the different tasks required to quantify the uncertainties in the storm surge forecast. The first task identifies the uncertain inputs and their probability distributions. Two scenarios with different perturbation parameters have been explored in this work: the first considers uncertainties in the hurricane track and intensity (i.e., perturbing $\varphi(t)$, $\lambda(t)$, and $v_{\max}(t)$) while the second keeps the track fixed but perturbs the hurricane intensity ($v_{\max}(t)$) and bottom drag parameters ($\mathsf{n}(\boldsymbol{x})$). Once the uncertain inputs are determined and parameterized, the second task is to sample the uncertain input space and to compute the corresponding model outputs. This step, often referred to as the *design of experiments* in forward-propagation problems, is performed via an ensemble calculation and is the most computationally demanding step. The next task concerns the construction and validation of a surrogate model. The difficulty for the PWL is to represent a random *field* efficiently: the surrogate constructed here combines spatial model reduction and stochastic functional representation and is described in Section 5. The sensitivity fields and exceedance probability maps are directly derived from the surrogates (see Section 6).

Algorithm 1 Overview of the implementation of the uncertainty quantification framework. The details of the implementation steps are provided in the sections.

4 Uncertain model inputs

The design of experiments in uncertainty quantification is not a trivial task. First, the user has to contend with the "uncertainties about the input uncertainties." For example, the ranges of the uncertain inputs and their probability density functions are seldom available from data but must be specified in order for the uncertainty quantification experiment to proceed. The specification of these uncertain input data must be informed by current forecast uncertainties to ensure that reasonable estimates of the output uncertainties are produced. A second challenge arises when dealing with time and/or space-dependent input quantities, as is the case here with the cyclonic pressure and wind fields, as well as the spatially varying bottom friction coefficient. A third recurring challenge in the construction of uncertainty experiments is the need to perturb the input data to account for the maximum amount of uncertainty while minimizing the number of uncertain inputs and producing realistic uncertainty scenarios. This section details the strategies that we have implemented to perturb the track and intensity of a hurricane along with the friction coefficients. As mentioned earlier, the control run uses the BT data to assign the hurricane track, size, and intensity, and the wind spatial distribution is determined by the Holland model. It is important to remember that the BT data are not the "true" hurricane properties as they are polluted by observational errors; the BT data, however, represent the best estimates available.

The paradigm adopted to assign input uncertainties to these storm properties is to compute their fluctuations within a specified time window and identify these fluctuations as perturbations to the control run with uncertain amplitudes (a zero amplitude perturbation would recover the BT data).

4.1 Best track data of Hurricane Gustav

The Holland model parameters for the control run were extracted from the National Hurricane Center (NHC) tropical cyclone report [3]. These consist of six-hourly BT data for the center latitude and longitude, central pressure, and maximum wind speed, the radius of maximum winds being reported in an Automated Tropical Cyclone Forecast (ATCF) format file [39]. More specifically, our baseline scenario used the BT data starting from 18h00 UTC on 28 August and the ensemble simulations start from the east coast of Jamaica on a deterministic position $(\varphi^0, \lambda^0) = (18°N, 76.2°W)$ (see Fig. 5). Accordingly, we remove the BT data prior to the starting date. As the radius of maximum winds vanishes one day after landfall when Gustav turns into a tropical depression, we also truncate the end of the intensity BT data after that date. In the following, the length N of the BT time series is equal to 32 for the track perturbations and 19 for the intensity perturbations.

4.2 Track uncertainties

The trajectory of the eye of a hurricane plays a central role since it controls the eye wall location, and hence the spatial distribution of winds and rainfall. Since the storm track and its forward speed are linked, we opt to perturb the hurricane's forward velocity and compute the ensuing trajectory; the hurricane velocity is estimated by finite differencing the latitudes and longitudes of the BT data.
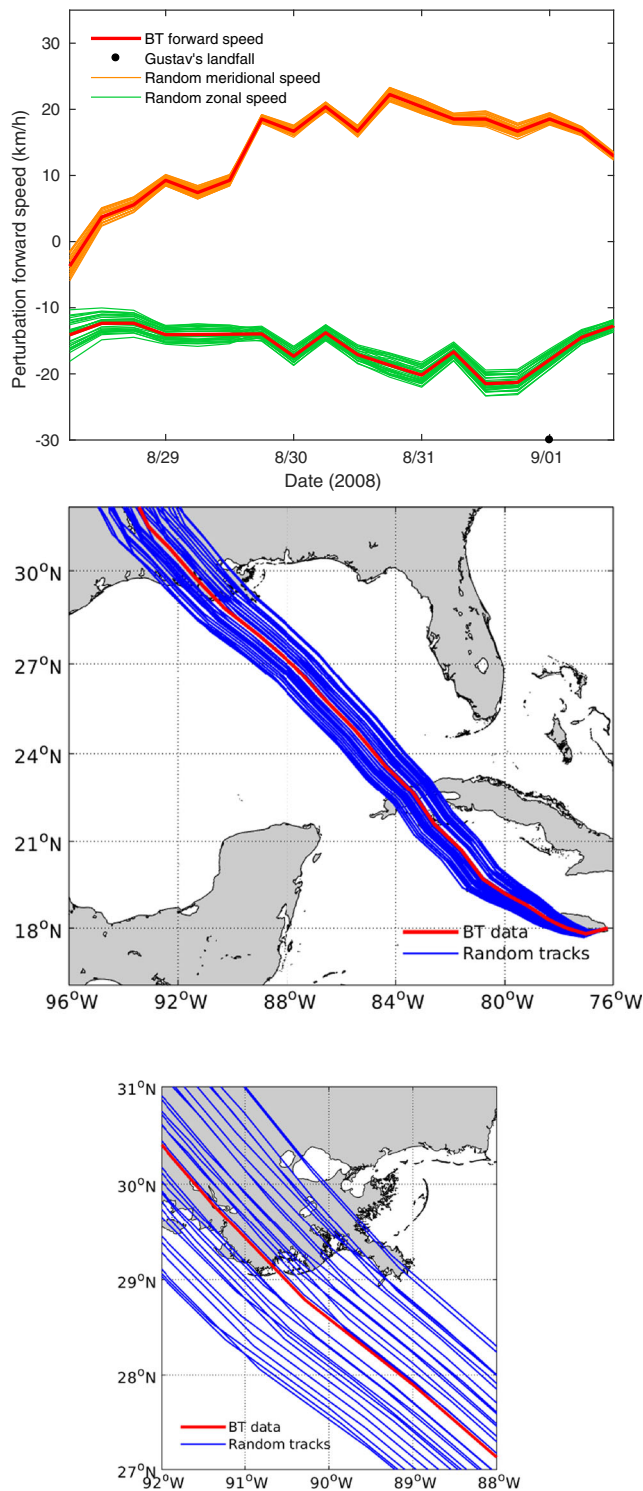
Let $V_{\mathrm{bt}} \in \mathbb{R}^{2,N}$ be the matrix collecting the meridional and zonal velocities reconstructed with the BT data. This matrix can be rewritten as

$$V_{\mathrm{bt}} = M_{V_{\mathrm{bt}}} + \Sigma_{V_{\mathrm{bt}}} V'_{\mathrm{bt}},$$

where $M_{V_{\mathrm{bt}}} \in \mathbb{R}^{2,N}$ is a matrix whose columns are the mean forward speed, $\Sigma_{V_{\mathrm{bt}}} \in \mathbb{R}^{2,2}$ is a diagonal scaling matrix with entries equal to the standard deviation, and $V'_{\mathrm{bt}} \in \mathbb{R}^{2,N}$ are standardized deviations (i.e., with zero mean and unit variance). As the two components of the forward speed are correlated, they need to be perturbed jointly. For that purpose, a singular value decomposition (SVD) is performed on the fluctuation part of V_{bt}

$$V_{\mathrm{bt}} = M_{V_{\mathrm{bt}}} + \Sigma_{V_{\mathrm{bt}}} U S W^\top, \tag{7}$$

where the triplet U, S, W comes from the SVD of V'_{bt}. The unitary matrix of left singular vectors $U \in \mathbb{R}^{2,2}$ couples the velocity components while the diagonal matrix of singular

Fig. 5 The top panel represents 30 realizations of the forward speed obtained with $\alpha = 0.15$ and uniform distributions for ξ_1 and ξ_2; the middle and bottom panels show the corresponding tracks over the Gulf of Mexico and Southeastern Louisiana. The BT data is shown in red

values $S \in \mathbb{R}^{2,2}$ scales the right singular vectors collected in the unitary matrix $W \in \mathbb{R}^{2,N}$ and representing the temporal fluctuations. We propose to modify the track by changing the velocity fluctuations as follows,

$$V_{uq}(\xi_1, \xi_2) = M_{V_{bt}} + \Sigma_{V_{bt}} U (I_2 + \alpha D(\xi_1, \xi_2)) S W^\top, \quad (8)$$

where $I_2 = [\delta_{i,j}]$ denotes the identity matrix ($\delta_{i,j}$ being the Kronecker delta) and $D(\xi_1, \xi_2) = [\xi_i \delta_{i,j}] \in \mathbb{R}^{2,2}$ a diagonal matrix. The forward velocity perturbation (8) depends on two random variables ξ_1 and ξ_2, as well as a multiplicative factor α. The $\xi_{i \in \{1,2\}}$ are assumed to have a zero mean in order to produce profiles whose mean corresponds to the observations. Indeed, using the reformulation

$$V_{uq}(\xi_1, \xi_2) = V_{bt} + \alpha \Sigma_{V_{bt}} U D(\xi_1, \xi_2) S W^\top, \quad (9)$$

we have $\mathbb{E}(V_{uq}) = V_{bt}$ if and only if $\mathbb{E}(D) = 0$. The factor $\alpha > 0$ is here introduced to control the amplitude of perturbations. The uncertain hurricane track is finally computed by integrating the velocities in time:

$$\varphi^{n+1}(\xi_1, \xi_2) = \varphi^n(\xi_1, \xi_2) + \frac{\delta t}{C_\varphi} v_{\varphi, uq}^n(\xi_1, \xi_2),$$

$$\lambda^{n+1}(\xi_1, \xi_2) = \lambda^n(\xi_1, \xi_2) + \frac{\delta t}{C_\lambda^n} v_{\lambda, uq}^n(\xi_1, \xi_2),$$

where $\delta t = 6$ h and the parameters $C_\varphi = 111.3$ and $C_\lambda^n = 111.3 \cos(\varphi^n)$ convert kilometers to degrees. The sets $\{v_{\varphi, uq}^n\}$ and $\{v_{\lambda, uq}^n\}$ are the coefficients of the matrix $V_{uq} \in \mathbb{R}^{2,N}$. In addition, the deterministic location of the starting point (φ^0, λ^0) initializes the random sequence $\{(\varphi^n(\xi_1, \xi_2), \lambda^n(\xi_1, \xi_2))\}_{1 \leq n \leq N}$. Thirty random realizations of the meridional and zonal velocities are plotted in Fig. 5 where the resulting uncertainty in the track can also be appreciated.

4.3 Intensity uncertainties

Three parameters characterize the intensity of the hurricane: the central pressure, the maximum wind, and the radius of maximum winds. These three parameters are correlated and an SVD procedure similar to the one used for the velocity can be used to identify the temporal fluctuations; this would result in an additional three uncertain parameters. However, to constrain the number of random variables and the ensuing ensemble size, the central pressure and the radius of maximum winds are kept fixed to the BT values, and we consider only the maximum wind to be uncertain as the latter contributes most to the hurricane intensity. The fluctuation part of the BT maximum wind $\boldsymbol{v}_{max, bt} \in \mathbb{R}^N$ is randomized according to

$$\boldsymbol{v}_{max, uq}(\xi_3) = \boldsymbol{v}_{max, bt} + \beta \sigma_{\boldsymbol{v}_{max, bt}} \xi_3 \boldsymbol{v}'_{max, bt}, \quad (10)$$

where $\boldsymbol{v}_{\mathrm{max,bt}}$ is the BT maximum wind, $\sigma_{\boldsymbol{v}_{\mathrm{max,bt}}}$ its standard deviation, and $\boldsymbol{v}'_{\mathrm{max,bt}}$ the standardized $\boldsymbol{v}_{\mathrm{max,bt}}$. As for the track perturbation, the distribution of the random variable ξ_3 is assumed to have a support over $[-1, 1]$ and the positive multiplicative factor β controls the amplitude of the perturbation. The uncertain versions of the cyclonic pressure and wind fields provided by the Holland model with a unitary shape parameter (see Eqs. 28 and 29 in Appendix) at the discrete times t^n are

$$p^n(r, \xi_3) = p_{\mathrm{c}}^n + \rho_{\mathrm{a}}(v_{\mathrm{max,uq}}^n(\xi_3))^2 \exp\left(-\left(R_{\mathrm{mw}}^n/r\right) + 1\right),$$
$$v^n(r, \xi_3) = v_{\mathrm{max,uq}}^n(\xi_3) \left[\left(R_{\mathrm{mw}}^n/r\right) \exp\left(-\left(R_{\mathrm{mw}}^n/r\right) + 1\right)\right]^{\frac{1}{2}},$$

where the set $\{v_{\mathrm{max,uq}}^n\}$ corresponds to the components of $\boldsymbol{v}_{\mathrm{max,uq}}$ while p_{c}^n and R_{mw}^n are given by the BT data. The triplet $(p_{\mathrm{c}}^0, v_{\mathrm{max}}^0, R_{\mathrm{mw}}^0)$ used to initialize the sequence are the BT data of the starting point. Figure 6 represents 30 realizations of the maximum wind speed where the coefficient β has been chosen to yield a maximum upper limit close to 270 km/h. The 30 landfall pressure and wind profiles stemming from these realization are also plotted.

Although the BT data are used as reference to generate the track and intensity realizations, the use of uniform distributions for ξ_1 and ξ_2 in Eq. 8 and ξ_3 in Eq. 10 yields equiprobable trajectories and maximum wind time series, respectively. This assumption can be straightforwardly modified; for instance, symmetrical beta or triangular distributions would lead to highest probabilities for the BT observations. Otherwise, the choice of the user-defined factors α and β is mostly one of convenience, these parameters controlling the amplitude of the perturbations, that is the width of the track uncertainty for α and the maximum wind speed amplitude for β. As a closing remark, the strength of our strategy is to provide a set of plausible hurricane realizations with a few random variables while its weakness is to use the BT data that are only available after a cyclonic event. Alternative options to get around this problem are discussed in Section 7.
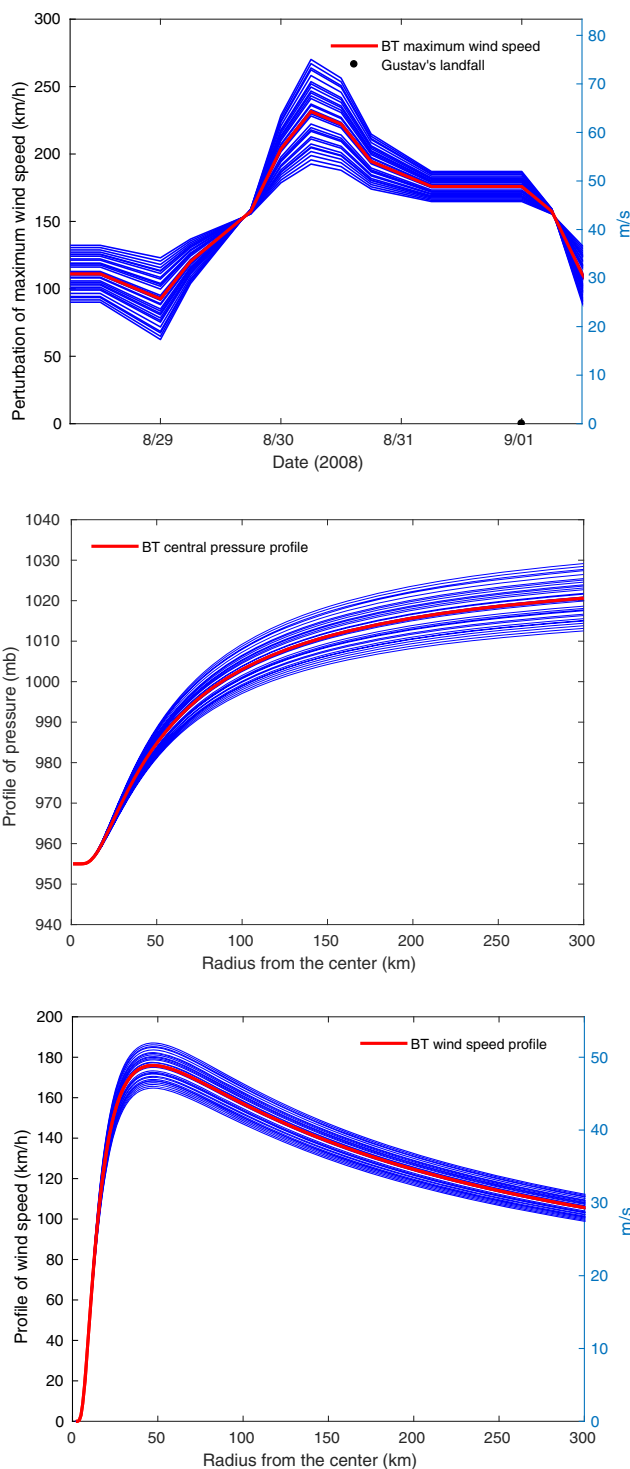
4.4 Manning coefficient

The Manning roughness coefficient $\mathsf{n}(\boldsymbol{x})$ in Eq. 4 is assumed to be piecewise uncertain on the east part Ω_{e} and the west part Ω_{w} of the Mississippi River,

$$\mathsf{n}(\boldsymbol{x}, \xi_1, \xi_2) = \mathsf{n}_{\mathrm{e}}(\xi_1) \mathbb{1}_{\Omega_{\mathrm{e}}}(\boldsymbol{x}) + \mathsf{n}_{\mathrm{w}}(\xi_2) \mathbb{1}_{\Omega_{\mathrm{w}}}(\boldsymbol{x}), \qquad (11)$$

where the $\mathbb{1}_{\Omega}(\boldsymbol{x})$ is the indicator function of Ω defined as 1 if $\boldsymbol{x} \in \Omega$ and 0 otherwise. The two Manning coefficients are modeled as

$$\mathsf{n}(\xi) = \frac{\xi}{2}\left(\mathsf{n}^{\mathrm{max}} - \mathsf{n}^{\mathrm{min}}\right) + \frac{1}{2}\left(\mathsf{n}^{\mathrm{max}} + \mathsf{n}^{\mathrm{min}}\right), \qquad (12)$$

Fig. 6 Thirty realizations of the maximum wind speed (top) for $\beta = 0.5$ and a uniform distribution of ξ_3. The corresponding landfall radial profiles for the pressure and wind speed are also shown (middle and bottom). The BT data are plotted in red

where n denotes n_{e} or n_{w} and ξ is distributed over $[-1, 1]$. Their minimal and the maximal values $\mathsf{n}^{\mathrm{min}}$ and $\mathsf{n}^{\mathrm{max}}$ are given in Table 4.

5 Surrogate construction

Our quantity of interest is the PWL during the storm event in the area of New Orleans. It is subjected to uncertain sources parameterized by a vector of $p = 3$ independent random variables $\boldsymbol{\xi} = (\xi_1, \cdots, \xi_p)$. We proceed in two steps to construct the surrogate: (i) a decomposition according to empirical orthogonal functions (EOF) to get a tractable number of spatial degrees of freedom, followed by (ii) a polynomial chaos (PC) expansion of the EOF coefficients to treat the stochastic part of the quantity of interest. This procedure, combining dimension reduction technique and spectral expansions, is an efficient practice [29] and is briefly outlined in this section.

The PWL random field $H(\boldsymbol{x}, \boldsymbol{\xi})$ is computed at the mesh nodes and we denote H($\boldsymbol{\xi}$) the random vector of the PWL at the $N_x = 130, 345$ nodes of the domain of interest. Separating the mean $\overline{\mathrm{H}}$, we get

$$H(\boldsymbol{\xi}) = \overline{\mathrm{H}} + \mathrm{H}'(\boldsymbol{\xi}), \text{ where } \overline{\mathrm{H}} = \frac{1}{N} \sum_{j=1}^{N} \mathrm{H}^{(j)}, \tag{13}$$

such that the fluctuation vector $\mathrm{H}'(\boldsymbol{\xi})$ is centered.

5.1 Empirical orthogonal functions

The computational burden related to the spatial dependency of the PWL can be handled using spatial correlations across the stochastic domain through the empirical orthogonal functions [31]. This decomposition uses the eigenpairs $\{\lambda_k, \mathrm{u}_k\}$ of the empirical spatial covariance matrix $\mathcal{C} \in \mathbb{R}^{N_x, N_x}$ satisfying

$$\mathcal{C}\mathrm{u}_k = \lambda_k \mathrm{u}_k, \quad \mathrm{u}_k \cdot \mathrm{u}_l = \delta_{k,l}, \tag{14}$$

where $\mathcal{C} = MM^\top/(N-1)$ with $M = [\mathrm{H}^{(i)'}] \in \mathbb{R}^{N_x, N}$ the matrix of fluctuations. By keeping the r main modes, we obtain the following EOF decomposition:

$$\mathrm{H}^r(\boldsymbol{\xi}) = \overline{\mathrm{H}} + \sum_{k=1}^{r} \zeta_k(\boldsymbol{\xi})\sqrt{\lambda_k}\mathrm{u}_k, \tag{15}$$

where $\zeta_k(\boldsymbol{\xi}) = \mathrm{H}'(\boldsymbol{\xi}) \cdot \mathrm{u}_k/\sqrt{\lambda_k}$ is the projection of the fluctuation onto the vector u_k. The truncation of the EOF decomposition is such that the r first modes retain a significant part of the spatial variability quantified by the ratio $\sum_{k=1}^{r} \lambda_k / \sum_{k=1}^{N} \lambda_k$, where the eigenvalues $\{\lambda_k\}$ are assumed to be ranked in descending order. As $N_x \gg N$ in our case study, we calculate more efficiently the eigenpairs of the matrix $\mathcal{C}$ by computing the eigenpairs $\{\lambda_k, \mathrm{w}_k\}$ of the matrix $\widetilde{\mathcal{C}} = M^\top M \in \mathbb{R}^{N, N}$ and deducing the desired eigenvectors as $\mathrm{u}_k = M\mathrm{w}_k\|M\mathrm{w}_k\|_2^{-1}$.

5.2 Polynomial chaos expansion

The set of random coefficients $\{\zeta_k(\boldsymbol{\xi})\}$ in the EOF decomposition need to be specified to complete the surrogate construction. If the coefficients ζ_k have finite variance, the polynomial chaos framework [15, 27] allows us to expand this quantity as a series of the form:

$$\zeta_k(\boldsymbol{\xi}) = \sum_{\boldsymbol{l} \in \mathcal{L}} \zeta_{k,\boldsymbol{l}}\phi_{\boldsymbol{l}}(\boldsymbol{\xi}) + \epsilon_{\mathcal{L}}(\boldsymbol{\xi}), \tag{16}$$

where $\{\phi_{\boldsymbol{l}}(\boldsymbol{\xi})\}_{\boldsymbol{l} \in \mathbb{N}^N}$ are the PC basis functions, $\{\zeta_{k,\boldsymbol{l}}\}_{\boldsymbol{l} \in \mathbb{N}^N}$ are the deterministic coefficients of the series, $\boldsymbol{l} \in \mathbb{N}^N$ is a multi-index, $\mathcal{L}$ is the set of multi-indices of the expansion, and $\epsilon_{\mathcal{L}}(\boldsymbol{\xi})$ is the truncation error. The basis functions are commonly chosen to be orthogonal w.r.t. the probability density function $p_{\boldsymbol{\xi}}(\boldsymbol{\xi})$ characterizing the distribution of the stochastic variables,

$$\int_{\varXi} \phi_{\boldsymbol{k}}(\boldsymbol{\xi})\phi_{\boldsymbol{l}}(\boldsymbol{\xi}) p_{\boldsymbol{\xi}}(\boldsymbol{\xi})\mathrm{d}\boldsymbol{\xi} = \delta_{\boldsymbol{k},\boldsymbol{l}}\|\phi_{\boldsymbol{k}}\|^2, \tag{17}$$

where $\|\phi_{\boldsymbol{k}}\|^2$ is the squared norm of the basis function. The basis functions are products of univariate Legendre polynomials when the random variables are uniformly i.i.d. The multi-index set is defined by a standard isotropic truncation w.r.t. a given maximal total degree d,

$$\mathcal{L}(d) = \{\boldsymbol{l} \in \mathbb{N}^N, |\boldsymbol{l}| \leq d\}.$$

So the PC basis dimension is $N_b = (p + d)!/(p!d!)$.

The series coefficients $\{\zeta_{k,\boldsymbol{l}}\}_{\boldsymbol{l} \in \mathbb{N}^N}$ can be determined by minimizing the size of the error, $\|\epsilon_{\mathcal{L}}(\boldsymbol{\xi})\|$. A number of different procedures are available for the task [23, 27], such as pseudo-spectral projection, least squares regression, and compressed sensing. These procedures differ mainly in the specific norm used to minimize the truncation error; they are implemented at the post-processing stage (online stage) of a non-intrusive approach via ensemble calculations (offline stage) without any changes to the storm surge model itself. We adopt a compressed sensing based approach here, the Basis Pursuit DeNoising (BPDN) [5], since it is particularly efficient when a limited number of simulations is available [23]. BPDN seeks to find the sparsest PC series that minimizes the sum of the squared distances to the ensemble realizations. Mathematically, it consists in solving the following minimization problem

$$\arg \min_{\boldsymbol{\zeta}_k} \left(\gamma \|\boldsymbol{\zeta}_k\|_1 + \|M\boldsymbol{\zeta}_k - \boldsymbol{\zeta}_k^{\mathrm{sim}}\|_2 \right), \tag{18}$$

where $M = [\phi_{\boldsymbol{l}}(\boldsymbol{\xi}^{(j)})] \in \mathbb{R}^{N, N_b}$ contains the N_b PC basis functions evaluated at the ensemble members, $\boldsymbol{\zeta}_k = [\zeta_{k,\boldsymbol{l}}]^\top \in \mathbb{R}^{N_b}$ collects the PC coefficients, and $\boldsymbol{\zeta}_k^{\mathrm{sim}} = [\zeta_k(\boldsymbol{\xi}^{(j)})]^\top \in \mathbb{R}^N$ contains the values of ζ_k associated with the simulations. The positive penalty parameter γ balances the original fitting problem with the regularization

one, while the l_1-norm ensures the sparsity of the PC expansion. We use an off-the-shelf algorithm [1, 2] to solve the optimization problem (18) with a leave-one-out cross-validation procedure to fit the penalty parameter.

Finally, substituting the exact EOF coefficients $\zeta_k(\boldsymbol{\xi})$ by their PC approximations $\zeta_k^{\mathcal{L}}(\boldsymbol{\xi})$ leads to the EOF-PC surrogate,

$$\mathrm{H}^{r,\mathcal{L}}(\boldsymbol{\xi}) = \overline{\mathrm{H}} + \sum_{k=1}^{r} \zeta_k^{\mathcal{L}}(\boldsymbol{\xi})\sqrt{\lambda_k}\mathrm{u}_k, \tag{19}$$

$$= \overline{\mathrm{H}} + \sum_{k=1}^{r} \sum_{l \in \mathcal{L}} \zeta_{k,l}\phi_l(\boldsymbol{\xi})\sqrt{\lambda_k}\mathrm{u}_k. \tag{20}$$

Once the truncation errors (due to the EOF and PC approximations) have been verified to be small, the surrogate (19) can be used in lieu of the model. The surrogate allows us to compute the statistical moments, determine the full pdf of the model output by drawing on a large number of samples, perform a sensitivity analysis, and estimate exceedance probability.

5.3 Global sensitivity analysis

An important goal of uncertainty quantification is to identify the relative contribution of each uncertain input parameter (or group of input parameters) to the variance of the output quantity. Assuming that the PWL random field has finite variance and that the model inputs $\boldsymbol{\xi}$ are independent, the variance of H can be decomposed [43] into

$$\mathbb{V}(H) = \sum_{i=1}^{p} \mathbb{V}_i + \sum_{i<j} \mathbb{V}_{i,j} + \cdots + \mathbb{V}_{1,\cdots,p}, \tag{21}$$

where $\mathbb{V}_i$ denotes the variance contributed by the uncertainty in the input parameter ξ_i only, $\mathbb{V}_{i,j}$ is the variance contributed by the combined effects of uncertainties in ξ_i and ξ_j (the so-called second-order interaction), and $\mathbb{V}_{i,\cdots,p}$ is the variance of the p-order interaction. The terms of Eq. 21 are divided by the variance to derive the sensitivity indices [20], the first-order terms leading to the Sobol indices,

$$S_i(H) = \frac{\mathbb{V}_i}{\mathbb{V}(H)}. \tag{22}$$

These indices are commonly used in order to rank the contributions of the different input uncertainty sources on the output. The index S_i increases as the influence of the uncertain input ξ_i on the output uncertainty increases; it thus quantifies the impact of the uncertainty in the ith input variable on the output uncertainty. More generally, higher order and total sensitivity indices can be defined to quantify the interaction effects among input parameters. The computation of such indices turns out to be unimportant

in the present application since we have observed that the uncertainty can be explained mainly by first-order indices.

We emphasize that the computation of global sensitivity indices is impractical for a costly model without a surrogate construction as it would require a prohibitive number of simulations (typically several hundred thousands). One primary advantage of a PC surrogate is the direct availability of the sensitivity indices which, owing to the orthogonality of the basis functions [6], now consist of a weighed sum of the PC coefficients. For example, the first-order sensitivity index of a PC expansion $H^{\mathcal{L}}(\boldsymbol{\xi}) = \sum_{l \in \mathcal{L}} H_l \phi_l(\boldsymbol{\xi})$ simply reads

$$S_i(H^{\mathcal{L}}) = \frac{\sum_{l \in \mathcal{L}_i} H_l^2 \|\phi_l\|^2}{\sum_{l \in \mathcal{L}^*} H_l^2 \|\phi_l\|^2}, \tag{23}$$

where $\mathcal{L}_i = \{l \in \mathcal{L},\ l_{j=i} > 0,\ \text{and}\ l_{j\neq i} = 0\}$ and $\mathcal{L}^* = \mathcal{L} \setminus \mathbf{0}$. Fields of sensitivity indices can be obtained with the EOF-PC surrogate rewriting (19) as

$$\mathrm{H}^{r,\mathcal{L}}(\boldsymbol{\xi}) = \overline{\mathrm{H}} + \sum_{l \in \mathcal{L}} \widetilde{\mathrm{H}}_l^r \phi_l(\boldsymbol{\xi}),\ \text{with}\ \widetilde{\mathrm{H}}_l^r = \sum_{k=1}^{r} \zeta_{k,l}\sqrt{\lambda_k}\mathrm{u}_k.$$

5.4 Exceedance probability

Coastal areas that are at risk of flooding under extreme tropical cyclones conditions can be identified using exceedance probability maps. Let H^+ be a threshold level, the probability of exceeding H^+ at the kth node $\boldsymbol{x}_k$ of the mesh is defined as

$$\mathbb{P}\left(H(\boldsymbol{x}_k, \boldsymbol{\xi}) > H^+\right) = \int_{\varXi} \mathbb{1}_{H(\boldsymbol{x}_k,\boldsymbol{\xi})>H^+}\ p_{\boldsymbol{\xi}}(\boldsymbol{\xi})\mathrm{d}\boldsymbol{\xi}, \tag{24}$$
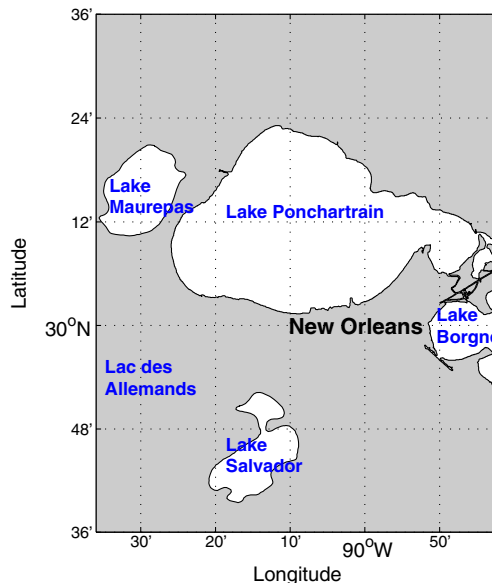

Fig. 7 Location of New Orleans and surrounding lakes into the target domain [29.6, 30.6]°N × [89.7, 90.6]°W

Table 1 First scenario: uncertain inputs and their extreme values on 08/30 (6pm) for $\alpha = 0.15$ and $\beta = 0.5$
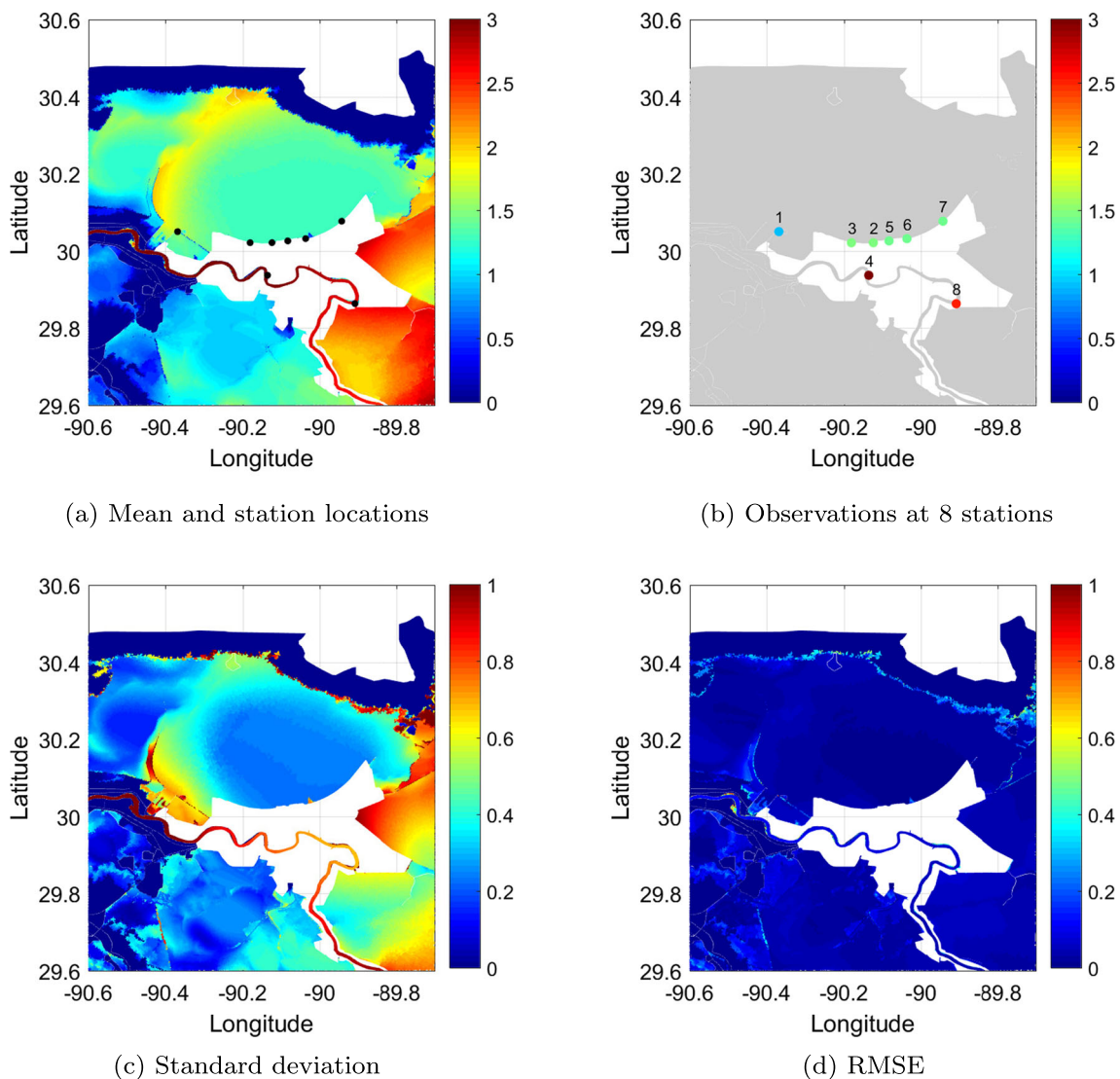
Quantities	Unit	Min	Max	RVs
$\varphi(t)$	°N	21.2	22.0	ξ_1, ξ_2
$\lambda(t)$	°W	81.9	83.2	ξ_1, ξ_2
$v_{max}(t)$	km/h	192	270	ξ_3

and is estimated by sampling the surrogate at $\mathcal{N}$ realizations $\{\boldsymbol{\xi}^{(j)}\}_{1 \le j \le \mathcal{N}}$ w.r.t. $p_{\boldsymbol{\xi}}(\boldsymbol{\xi})$ and calculating

$$\mathbb{P}\left(\mathrm{H}_k^{r,\mathcal{L}}(\boldsymbol{\xi}) > H^+\right) = \frac{1}{\mathcal{N}} \sum_{j=1}^{\mathcal{N}} \mathbb{1}_{\mathrm{H}_k^{r,\mathcal{L}}(\boldsymbol{\xi}^{(j)}) > H^+}. \quad (25)$$

6 Results

We investigate two uncertainty scenarios in the sections below that focus on different subsets of the uncertain input data, namely either uncertainties in the hurricane track and intensity or uncertainties in the hurricane intensity and the bottom friction coefficient. This sequence of experiments was designed to separate the primary and secondary contributors to the storm surge forecast uncertainty. In addition, this sequential approach allowed us to reduce the size of the ensemble necessary for building an accurate surrogate. A single scenario including all the input uncertainty sources at the same time can obviously be designed but the required ensemble size increases quickly

(a) Mean and station locations

(b) Observations at 8 stations

(c) Standard deviation

(d) RMSE

Fig. 8 First scenario: empirical mean and standard deviation of the PWL obtained by merging the 150 realizations of the training and validation sets. The observations at some NOAA and USGS stations and the RMSE of the EOF-PC surrogate ($d = 10$) are also shown. New

Orleans is represented by the white area inside the different results maps and is assumed a non-flooded zone owing to the levee system of the town. The domain has 250,916 triangular elements and N_x=130,345 nodes

Table 2 Names of the stations used in Fig. 8b. Data at the NOAA station are referenced to mean sea level (MSL) and data at the USGS stations are referenced to the geodetic NAVD88 datum

No.	Station name
1	NOAA 8762372, East Bank 1
2	USGS SSS-LA-JEF-005
3	USGS SSS-LA-JEF-013
4	USGS SSS-LA-ORL-001
5	USGS SSS-LA-ORL-005
6	USGS SSS-LA-ORL-010
7	USGS SSS-LA-ORL-014
8	USGS SSS-LA-PLA-004

with the number of uncertain input data (a.k.a. the curse of dimensionality) and can become prohibitive especially for computationally expensive model such as ADCIRC.

The construction of the EOF-PC surrogate for each test scenario relies on $N = 100$ ADCIRC simulations that sample the uncertain parameter space according to a quasi-Monte Carlo method with a Halton sequence [36]. An independent validation set of $N^* = 50$ Monte-Carlo simulations is also used to assess the surrogate's accuracy. The domain of interest, shown in Fig. 7, is an area covering the city of New Orleans with the surrounding lakes, namely Lake Pontchartrain, Lake Borgne, Lake Maurepas, Lake Salvador and Lac des Allemands.
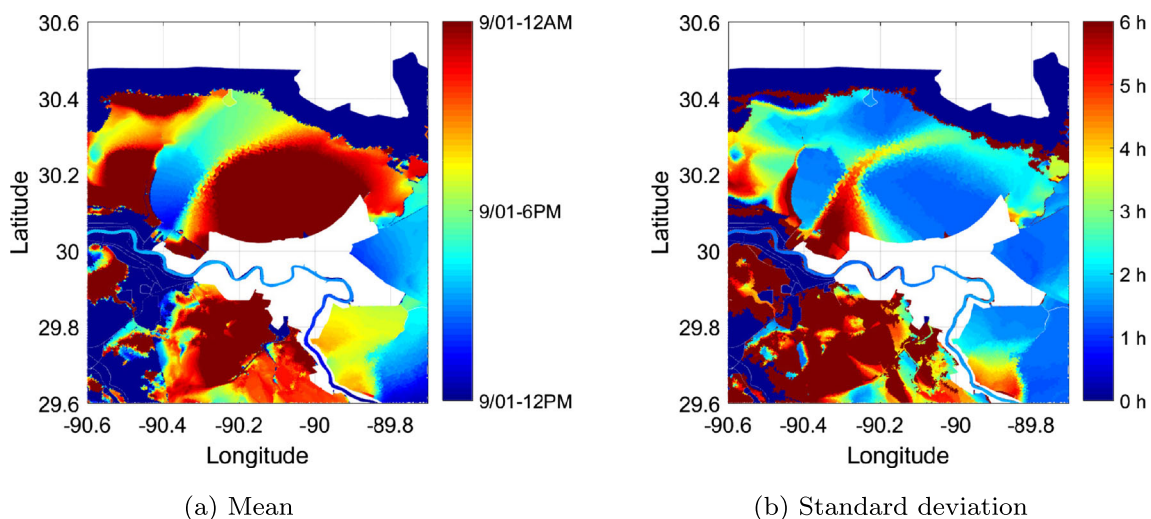
6.1 First test scenario

The two sources of uncertainty in the first test scenario stem from the track and intensity of the hurricane. Specifically, the latitude $\varphi(t)$ and longitude $\lambda(t)$ of the eye and the

maximum wind speed are parametrized by three uniformly i.i.d random variables, $\xi_i \sim \mathcal{U}([-1, 1])$, summarized in Table 1. Note that the type of input distributions can be changed retroactively, using the same ensemble, if the surrogate is sufficiently accurate.

6.1.1 Empirical moments

The PWL empirical mean plotted in Fig. 8a shows regions of highs and lows. We observe that the level in the Mississippi River and in the east part of the city is the largest (greater than 2 m), followed by the level in Lake Pontchartrain (located at the north of the city) and in the south part of the city (1–1.5 m). The north part of the lake and some areas in the southwest part of the city remain dry during the storm event. In order to gauge the realism of our ensemble, Fig. 8b shows observed PWL collected at eight NOAA and USGS stations listed in Table 2. The observed PWL can be classified into the three aforementioned groups: (i) a high level (beyond 2.5 m) in the Mississippi River (stations 4 and 8), (ii) a moderate level (around 1.5 m) in the north part of the city (stations 2, 3, 5, 6, and 7), (iii) a low level (lower than 1 m) in the northwest part of the city (station 1). The mean PWL field is thus broadly consistent with observational data. Station 1 is located in a zone of large gradients in PWL and the observed level is lower than the ensemble mean but still within a standard deviation. The standard deviation in Fig. 8c has roughly the same behavior as the mean with a high deviation in the Mississippi River and in the east part of the city. A zone with a standard deviation in the range [0.5, 1] m also appears in the southwestern part of Lake Pontchartrain.

The empirical moments of the storm arrival times are shown in Fig. 9. Regions of high PWL, namely the

(a) Mean

(b) Standard deviation

Fig. 9 First scenario: empirical mean and standard deviation of the PWL time of arrival obtained by merging the 150 realizations of the training and validation sets

Mississipi River and the east part of the city, are the first impacted while the other regions are hit later. Figure 9b shows that the uncertainty in the arrival time is low in regions of high PWL (standard deviation of about 1 h) whereas it is more uncertain in regions of low PWL (standard deviation up to 6 h). As for the PWL, a PC surrogate for the PWL arrival time can be built and mined for more detailed statistical information.

6.1.2 Surrogate validation

For the construction of the EOF-PC surrogate, we keep the first 24 EOF modes to capture 99% of the spatial variability. The parameter in the BPDN problem (18) minimizes the leave-one-out cross-validation error evaluated at 60 points logarithmically spaced over the interval $[10^{-1}, 10^2]$. Before exploiting the statistical information provided by the surrogate, it is necessary to check its accuracy. The space-dependent root-mean-square error, estimated with the validation set,

$$\text{RMSE} = \left[\frac{1}{N^*} \sum_{j=1}^{N^*} \left(\text{H}^{(j)} - \text{H}^{r,\mathcal{L}}(\boldsymbol{\xi}^{(j)}) \right)^2 \right]^{\frac{1}{2}}, \quad (26)$$
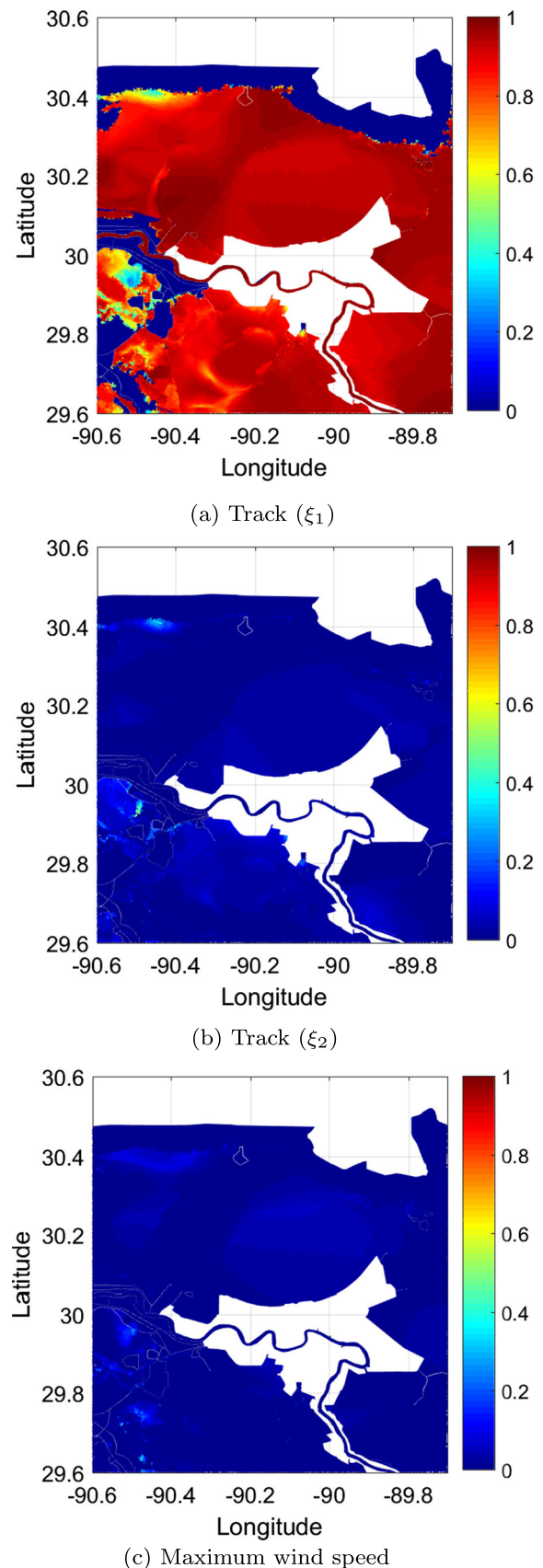
is plotted in Fig. 8d with the same scale as for the standard deviation and a maximal total degree equal to 10. The RMSE is much lower than the standard deviation, justifying the substitution of the direct model by the EOF-PC surrogate especially for the variance-based sensitivity analysis. The space-integrated mean squared error

$$\text{MSE} = \sum_{k=1}^{N_x} w_k \text{RMSE}_k^2, \quad (27)$$

where w_k (resp. RMSE_k) is the area weight (resp. the RMSE) of the kth finite element node in the integration, is reported in Table 3. Three truncation orders (5, 10, and 15) are considered to evaluate the effect of the PC series' length on the error. The MSE, whose unit is $[\text{m}^2 \times \text{km}^2]$, is low given that the surface area of the domain of interest is 7097 km^2. As expected, the error reaches a limit when the polynomial degree increases, additional simulations would be necessary to decrease the error further. The results presented hereafter are therefore obtained for $d = 10$.
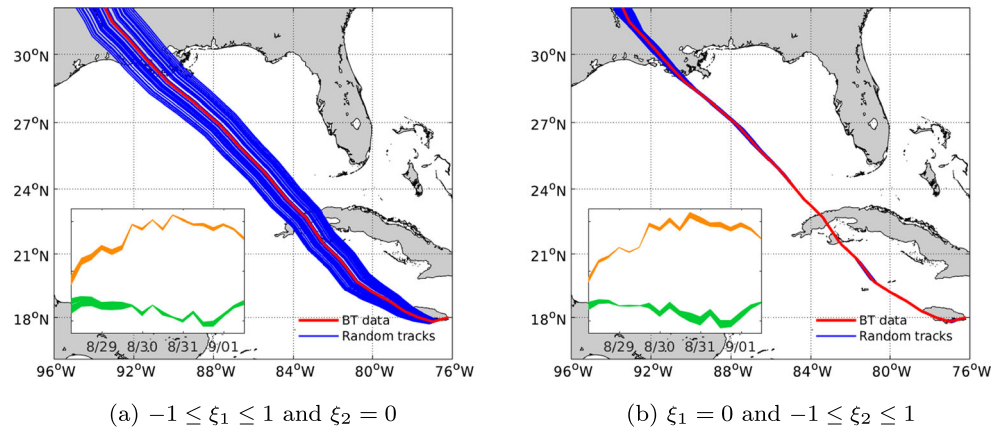
Table 3 Space-integrated MSE of the EOF-PC surrogate for the two scenarios

Scenario 1			Scenario 2		
d	N_b	MSE	d	N_b	MSE
5	56	38.62	2	10	8.68
10	286	29.51	5	56	6.43
15	816	29.03	10	286	6.41

(a) Track (ξ_1)

(b) Track (ξ_2)

(c) Maximum wind speed

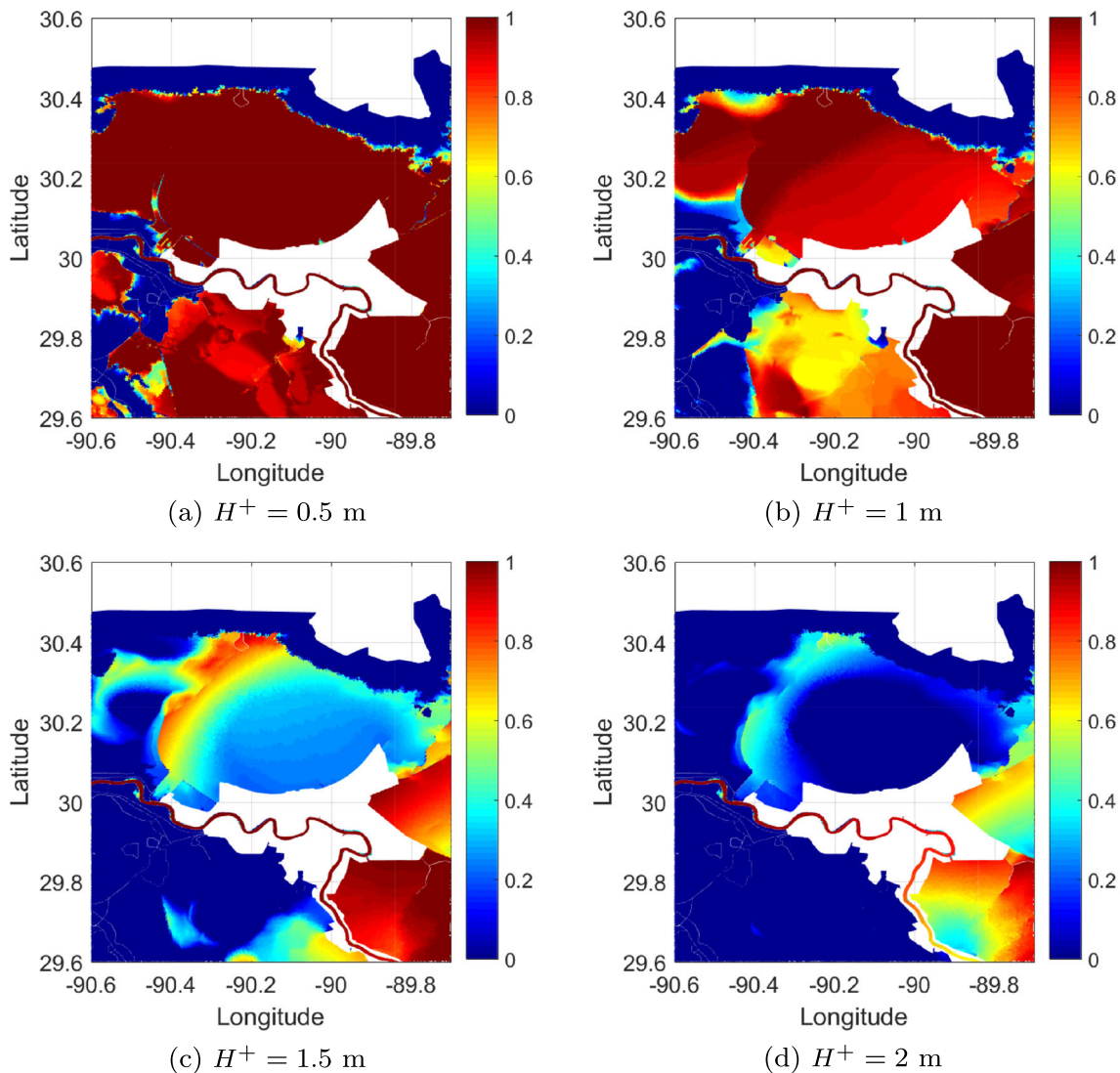**Fig. 10** First scenario: first-order sensitivity fields of the PWL

Fig. 11 30 realizations of the track with one-at-a-time (OAT) variation of ξ_1 (left) and ξ_2 (right). Plotted are the 30 associated realizations of the meridional (orange profiles) and zonal (green profiles) speeds in the internal boxes. Variations in ξ_1 leads to larger perturbations in the forward velocity components prior to 08/30 than variations in ξ_2

(a) $-1 \leq \xi_1 \leq 1$ and $\xi_2 = 0$

(b) $\xi_1 = 0$ and $-1 \leq \xi_2 \leq 1$

6.1.3 Sensitivity fields

The first-order sensitivity fields derived from the EOF-PC surrogate (see Section 5.3) are depicted in Fig. 10. All the variance in the PWL is contributed by the track perturbation through the first random variable ξ_1 only, whereas the other two uncertain inputs contribute very little as their first-order sensitivity indices are close to zero. There are negligible

(a) $H^+ = 0.5$ m

(b) $H^+ = 1$ m

(c) $H^+ = 1.5$ m

(d) $H^+ = 2$ m

Fig. 12 First scenario: storm surge exceedance probability maps for different values of the threshold obtained with a LHS of 10^5 realizations

interaction effects on the storm surge uncertainty since the sum of the indices (not shown here) is close to one, except in the area of Lac des Allemands.

To investigate the role of the random variable ξ_2, we analyze the track changes caused by varying only one of the uncertain track variables at a time; the results are shown in Fig. 11. The variations of ξ_1 (with ξ_2 fixed) produce diverging tracks spreading about 100 km on either side of the BT, while tracks due to ξ_2-variations (with ξ_1 fixed) cluster tightly around the BT trajectory. This difference in tracks is due to the early and larger perturbations to the forward speed (plotted in the internal boxes) caused by ξ_1 variations than those caused by ξ_2 variations (08/29-30). These ξ_1 perturbations lead to the formation of a "cone of uncertainty" that starts over Jamaica, as seen in Fig. 11a, while no cone forms when ξ_2 is varied in Fig. 11b.
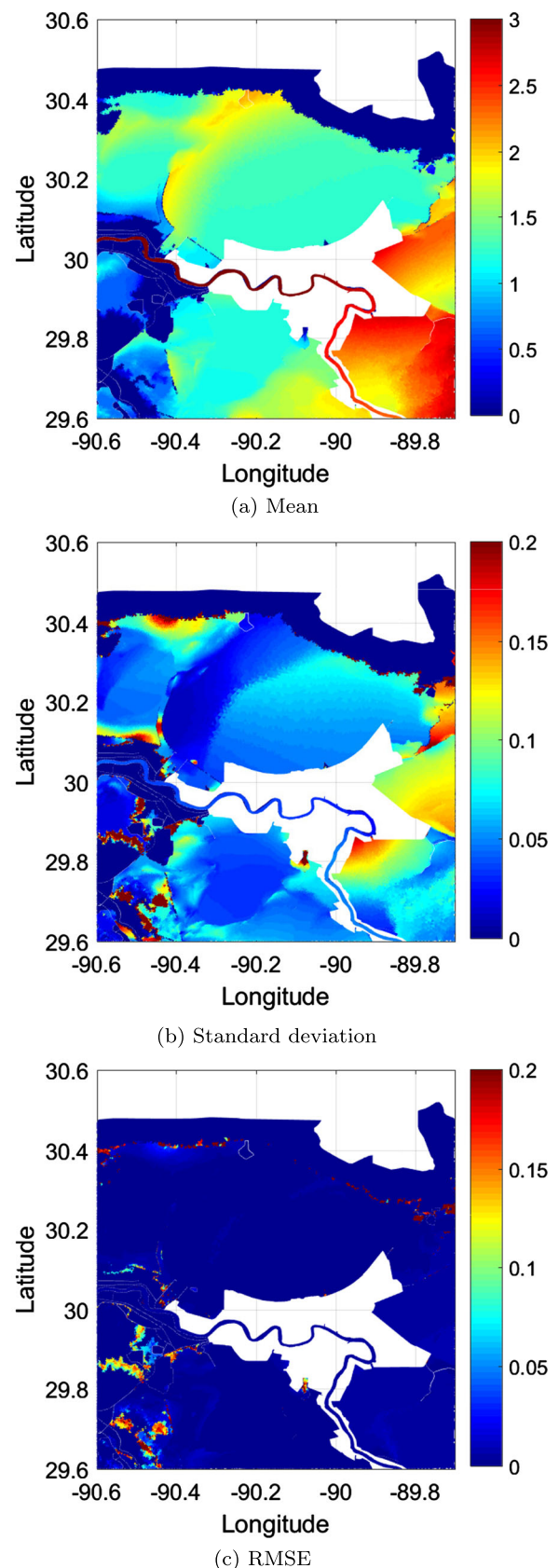
6.1.4 Exceedance probability maps

Figure 12 presents the exceedance probabilities, Eq. 25, computed using a Latin hypercube sampling (LHS) of 10^5 realizations (the differences with a LHS of size 10^4 are smaller than 1%). We can observe in Fig. 12a that a storm surge of at least 50 cm is inescapable for the entire area. The probabilities stay high for a 1 m storm surge in Fig. 12b; the exceedance probabilities decrease as the threshold increases. Figure 12 c and d show that the most vulnerable areas to larger storm surges (1.5 m and 2 m, respectively) are in the east part of the city and in the Mississippi River; this is consistent with the mean map in Fig. 8a.

6.2 Second test scenario

The second test scenario investigates the impacts of uncertainties in the hurricane intensity (via the maximum wind speed) and bottom friction coefficients on the storm surge forecast when the hurricane track is fixed. Table 4 lists the three uncertainty sources with their ranges. The perturbations of the maximum wind speed remain as prescribed in the first test scenario; while ξ_1 and ξ_2 described the uncertainty in Manning's coefficients over marshland and forested areas, respectively. The random

Table 4 Second scenario: uncertain inputs and the extreme values

Quantities	Unit	Min	Max	RVs
n_e	s/m$^{1/3}$	0.035	0.06	ξ_1
n_w	s/m$^{1/3}$	0.06	0.15	ξ_2
$v_{max}(t)$	km/h	192	270	ξ_3

(a) Mean

(b) Standard deviation

(c) RMSE

Fig. 13 Second scenario: empirical mean and standard deviation of the PWL and RMSE of the EOF-PC surrogate ($d = 5$)

variables $\{\xi_i\}$ are considered uniformly i.i.d over $[-1, 1]$ as in the previous case.

6.2.1 Empirical moments

The PWL empirical mean in Fig. 13a looks like the mean of the previous scenario except in the south part of the city where a higher level is observed. In contrast, the standard deviation, shown in Fig. 13b is different from the one in the previous scenario (Fig. 8c). First, the variation range is considerably reduced: [0, 20] cm instead of [0, 1] m, indicating a higher confidence in the forecasted PWL. Second, the zones with high standard deviations (large uncertainty in the PWL forecast) have changed: they now include an area between Lake Maurepas and Lake Pontchartrain, an area in the southeast part of the city close to the Mississippi River, and small patches in the southwest part of the city. Third, the standard deviation in the Mississippi River is small indicating low uncertainty in this forecast scenario. As for the PWL, the following conclusions about the first moments of the PWL time of arrival (not shown) can be drawn: the pattern of the mean is similar to the pattern of the first scenario (Fig. 9a) and the range of the standard deviation is minor.

6.2.2 Surrogate validation

The EOF-PC surrogate construction retained the first 31 EOF modes to capture 95% of the spatial variability. PC expansions of degree five have been selected and the same procedure used previously has been applied to fit the parameter in the BPDN. The RMSE (26) estimated with the 50 realizations of the validation set is shown in Fig. 13c. The error is close to zero except for small patches where the error still remains lower than the standard deviation. The MSE (27) is reported in Table 3 for three truncation orders (2, 5, and 10) in the PC series justifying the use of fifth-order PC expansions for subsequent analysis.

6.2.3 Sensitivity fields

Figure 14 displays the three first-order sensitivity fields related to the PWL variance decomposition. Figure 14a highlights that the uncertainty in the wind speed contributes the most to the uncertainty in the storm surge forecast in the wet zones that include Lake Pontchartrain, Lake Borgne, and Lake Salvador. On the other hand, Fig. 14b and c show that the uncertainties in the bottom friction coefficients influence the storm surge forecast uncertainty in the marshland and the forested zones. The situation is different in Lake Maurepas and in the southeast part of the city where the uncertainty in the maximum wind speed and the Manning coefficient contribute equally to
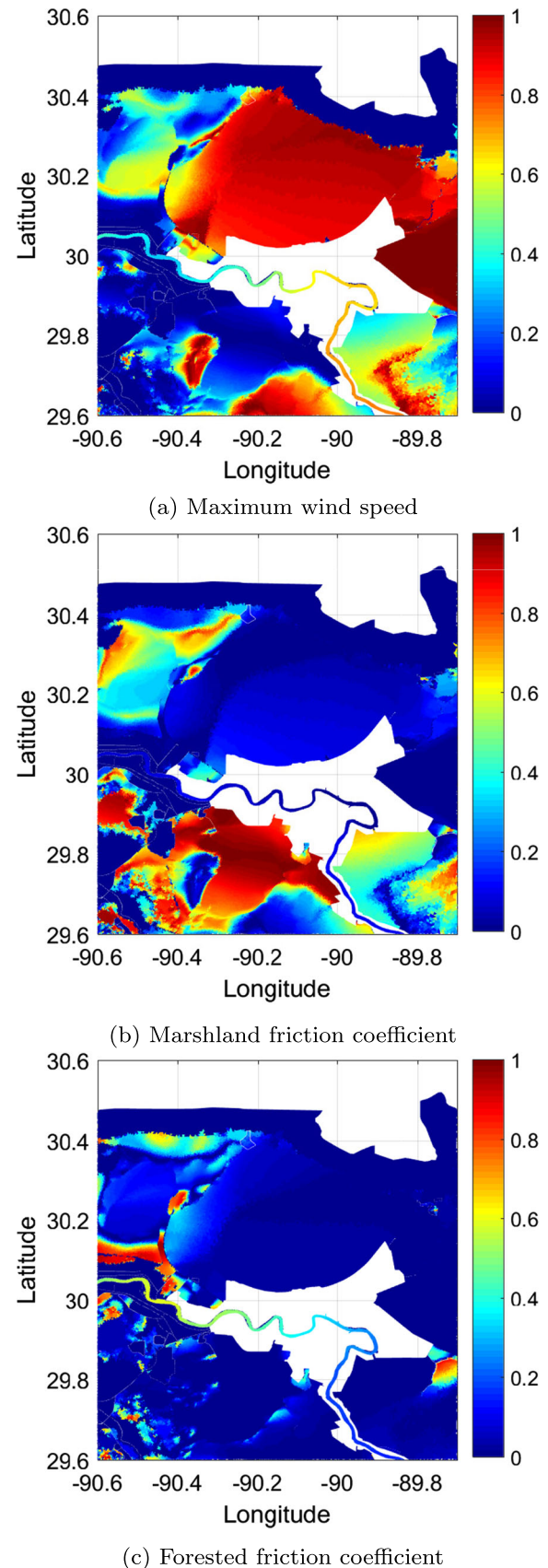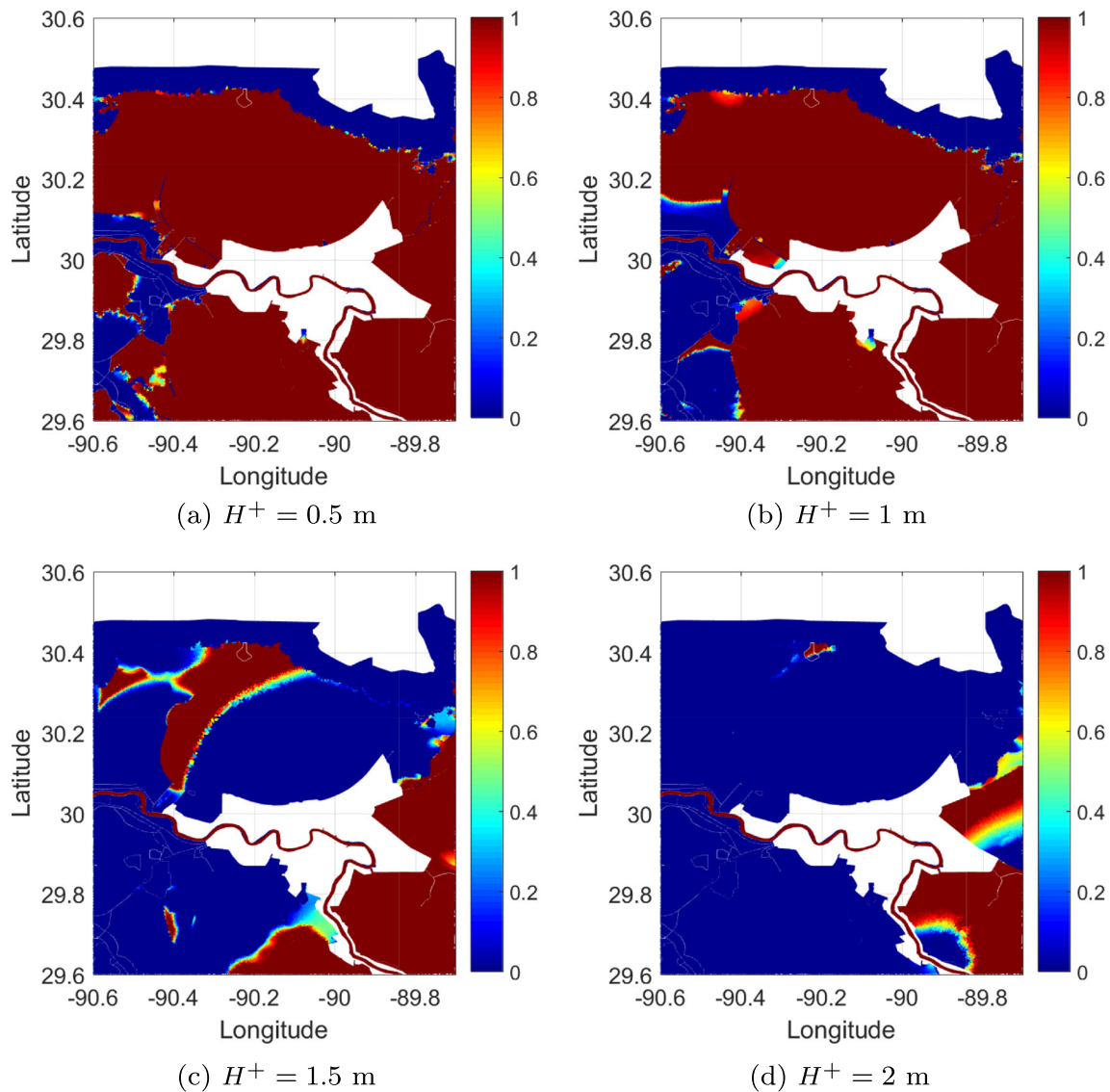

(a) Maximum wind speed

(b) Marshland friction coefficient

(c) Forested friction coefficient

Fig. 14 Second scenario: first-order sensitivity fields of the PWL

(a) $H^+ = 0.5$ m

(b) $H^+ = 1$ m

(c) $H^+ = 1.5$ m

(d) $H^+ = 2$ m

Fig. 15 Second scenario: storm surge exceedance probability maps for different values of the threshold obtained with a LHS of 10^5 realizations

the uncertainty in the storm surge forecast. Again, the interaction effects between the uncertain inputs (not shown here) are low compared with the first-order effects.

6.2.4 Exceedance probability maps

The four storm surge exceedance probability maps represented on Fig. 15 exhibit less nuanced responses than for the previous case in the sense that the probability of exceeding a given surge is almost binary here, either zero or unitary probabilities. Figure 15b shows that a PWL of at least 1 m is predicted over the domain of interest (except inside the city). Figure 15 c and d display that specific areas are subjected to higher storm surge: the south part of the city, the northwest part of Lake Pontchartrain and Lake Maurepas

with a level of 1.5 m as well as the east part of the city and the Mississippi River with a level of 2 m.

7 Conclusion

The present article formulated an uncertainty quantification framework for storm surge predictions based on a polynomial chaos surrogate approach. The surrogate is essentially an orthogonal series that provides an accurate and efficient approximation to changes to the model output in response to changes in the model inputs; it permits the statistical analysis to be performed properly. The surrogate is built using ensemble calculations and without modification of the forecast model.

The approach was illustrated by applying the methodology to forecasting the storm surge associated with Hurricane Gustav using ADCIRC as a forward model. The ADCIRC uncertain inputs included the meteorological forcing, namely the hurricane track and its maximum wind speed, along with uncertain frictional coefficients in marshland and forested areas. The input uncertainties were realized as perturbations to a control run where the input data consist of the observed BT data and unperturbed frictional coefficients. The parameters controlling the input data perturbations were considered uniformly distributed. The forward propagation of the input uncertainties was performed using a combination of empirical orthogonal functions for dimensionality reduction and polynomial chaos expansions. Two uncertainty quantification experiments were performed in order to reveal the relative influence of the uncertain inputs on the output uncertainties: a track and wind speed uncertainty experiment, and a wind speed and frictional coefficient uncertainties experiment where the track was held fixed. In both instances, the surrogate constructed for the peak water level was tested for accuracy using an independent set of forward model realizations. The sensitivity analyses highlight that the hurricane track is the prime contributor to the uncertainty in the peak water level forecast with the remaining parameters playing a secondary role. This result confirms that efforts must be concentrated mainly on the trajectory of the tropical cyclone in real-life weather forecasting. Hazards mapping emphasizes that the level of storm surge risk strongly depends on the location of interest and the storm event scenario. From a practical viewpoint, this type of statistical information, obtained with a tractable number of simulations, can be useful to construct and/or update storm surge planning zones and to design early warning systems for coastal populations.

The extension of our framework to real-time forecasting raises a number of questions. First, the methodology needs to be applied to different hurricanes to assess its performance under different conditions. Second, the specification of the track and wind perturbations in the absence of the BT data must be revisited. Several alternative options can be considered. A first option is to define a most probable track (for instance through the NHC track forecast cone) as BT track in order to apply our strategy based on a perturbation of the time series fluctuations. An alternative would be to utilize directly the tracks coming from different models (such as spaghetti models) as credible independent realizations of the trajectory. These options can be applied to produce uncertain time series of maximum wind speed.

Various aspects of this work can be improved in terms of physical model, inputs, and outputs. A more complex ocean model can be employed to account for the effects of waves, tides, and barometric pressure and a more realistic wind field could replace the Holland model. In addition to a higher computational burden, these extensions also require the implementation of an appropriate perturbation strategy of the input fields. With regards to the quantity of interest, it would be valuable to enrich the study of the maximum water level by investigating the dynamical aspect of the storm surge.

Appendix: Holland model

This parametric model [19] describes a symmetrical vortex and is derived by starting with an empirical analytical pressure field and by using the gradient wind equation to get the wind speed profile. The pressure field p is assumed to have an exponential profile,

$$p(r, t) = p_c(t) + (p_a(t) - p_c(t)) \exp\left(- (R_{mw}(t)/r)^B\right), \quad (28)$$

where r is the radial distance from the eye, t the time variable, $p_c(t)$ the central pressure, $p_a(t)$ the ambient pressure (at infinite radius), $R_{mw}(t)$ the maximum wind radius (RMW), and B the Holland parameter. Plugging the pressure profile (28) into the gradient wind equation [21] and neglecting the Coriolis force (assumed to be small in the region of maximum winds) leads to the following tangential wind speed profile,

$$v(r, t) = v_{max}(t) \left[(R_{mw}(t)/r)^B \exp\left(- (R_{mw}(t)/r)^B + 1\right)\right]^{\frac{1}{2}}, \quad (29)$$

where the maximum wind speed $v_{max}(t)$ has been introduced. This latter quantity is defined as $v(r = R_{mw}, t) = (B(p_a(t) - p_c(t))/(\rho_a e))^{1/2}$ with $\rho_a = 1.18 \text{kg/m}^3$ the air density, and $e = 2.72$ the Euler's number. Assuming that the central pressure and the maximum wind speed are known, the ambient pressure in Eq. 28 is then computed with $p_a(t) = p_c(t) + \rho_a e v_{max}^2(t)/B$. The shape parameter B of the model determines the steepness of the eyewall and the strength of the winds far from the center. Its value ranges over the interval $[0.5, 2.5]$ as mentioned in [49] and we set $B = 1$.

References

1. Berg, E.V.D., Friedlander, M.P.: SPGL1: a solver for large-scale sparse reconstruction. [Available online at http://www.cs.ubc.ca/labs/scl/spgl1] (2007)

2. Berg, E.V.D., Friedlander, M.P.: Probing the Pareto frontier for basis pursuit solutions. SIAM J. Sci. Comp. **31**(2), 890–912 (2008). https://doi.org/10.1137/080714488. http://link.aip.org/link/?SCE/31/890

3. Beven, J.L. II., Kimberlain, T.B.: Tropical cyclone report - hurricane Gustav. Tech. rep., National Oceanic and Atmospheric Administration/NHC. [Available online at http://www.nhc.noaa.gov/data/tcr/AL072008_Gustav.pdf] (2009)

4. Brown, J.D., Spencer, T., Moeller, I.: Modeling storm surge flooding of an urban area with particular reference to modeling uncertainties: a case study of Canvey Island, United Kingdom. Water Resour. Res. **43**(6). https://doi.org/10.1029/2005WR004597. https://agupubs.onlinelibrary.wiley.com/doi/abs/10.1029/2005WR004597 (2007)

5. Chen, S.S., Donoho, D.L., Saunders, M.A.: Atomic decomposition by basis pursuit. SIAM J. Sci. Comp. **20**, 33–61 (1998)

6. Crestaux, T., Le Maître, O., Martinez, J.M.: Polynomial chaos expansion for sensitivity analysis. Reliab. Eng. and Syst. Saf. **94**(7), 1161–1172 (2009)

7. Cruz-Jiménez, H., Li, G., Mai, P., Hoteit, I., Knio, O.: Bayesian inference of earthquake rupture models using polynomial chaos expansion. Geosci. Model Dev. **11**(7), 3071–3088 (2018). https://doi.org/10.5194/gmd-11-3071-2018. https://www.geosci-model-dev.net/11/3071/2018/

8. Dietrich, J.C.: Coauthors: a high-resolution coupled riverine flow, tide, wind, wind wave, and storm surge model for Southern Louisiana and Mississippi. Part II: synoptic description and analysis of hurricanes Katrina and Rita. Mon. Weather Rev. **138**(2), 378–404 (2010). https://doi.org/10.1175/2009MWR2907.1

9. Dietrich, J.C.: Coauthors: hurricane Gustav (2008) waves and storm surge: hindcast, synoptic analysis, and validation in Southern Louisiana. Mon. Weather Rev. **139**(8), 2488–2522 (2011). https://doi.org/10.1175/2011MWR3611.1

10. Elsheikh, A.H., Hoteit, I., Wheeler, M.F.: Efficient Bayesian inference of subsurface flow models using nested sampling and sparse polynomial chaos surrogates. Comput. Methods Appl. Mech. Engrg. **269**, 515–537 (2014). https://doi.org/10.1016/j.cma.2013.11.001. http://www.sciencedirect.com/science/article/pii/S004578251300296X

11. Finocchio, P.M., Majumdar, S.J., Nolan, D.S., Iskandarani, M.: Idealized tropical cyclone responses to the height and depth of environmental vertical wind shear. Mon. Weather Rev. **144**(6), 2155–2175 (2016). https://doi.org/10.1175/MWR-D-15-0320.1

12. Flowerdew, J., Horsburgh, K., Wilson, C., Mylne, K.: Development and evaluation of an ensemble forecasting system for coastal storm surges. Quart. J. Roy. Meteor. Soc. **136**(651), 1444–1456 (2010). https://doi.org/10.1002/qj.648. https://rmets.onlinelibrary.wiley.com/doi/abs/10.1002/qj.648

13. Forbes, C., Luettich, R.A. JR., Mattocks, C.A., Westerink, J.J.: A retrospective evaluation of the storm surge produced by hurricane Gustav. Forecast and Hindcast Results. Weather Forecast. **25**(6), 1577–1602 (2010). https://doi.org/10.1175/2010WAF2222416.1 (2008)

14. Formaggia, L., Guadagnini, A., Imperiali, I., Lever, V., Porta, G., Riva, M., Scotti, A., Tamellini, L.: Global sensitivity analysis through polynomial chaos expansion of a basin-scale geochemical compaction model. Comput. Geosci. **17**(1), 25–42 (2013). https://doi.org/10.1007/s10596-012-9311-5

15. Ghanem, R.G., Spanos, S.D.: Stochastic Finite Elements: a Spectral Approach. Springer, Berlin (1991)

16. Giraldi, L., Le Maître, O., Mandli, K., Dawson, C., Hoteit, I., Knio, O.: Bayesian inference of earthquake parameters from buoy data using a polynomial chaos-based surrogate. Comput. Geosci. **21**(4), 683–699 (2017). https://doi.org/10.1007/s10596-017-9646-z

17. Graham, L., Butler, T., Walsh, S., Dawson, C., Westerink, J.J.: A measure-theoretic algorithm for estimating bottom friction in a coastal inlet: case study of bay St. Louis during hurricane Gustav. Mon. Weather Rev. **145**(3), 929–954 (2017). https://doi.org/10.1175/MWR-D-16-0149.1

18. Heaps, N.S.: Storm surges, 1967–1982. Geophys. J. Roy. Astro. Soc. **74**(1), 331–376 (1983). https://doi.org/10.1111/j.1365-246X.1983.tb01883.x. https://onlinelibrary.wiley.com/doi/abs/10.1111/j.1365-246X.1983.tb01883.x

19. Holland, G.J.: An analytic model of the wind and pressure profiles in hurricanes. Mon. Weather Rev. **108**(8), 1212–1218 (1980). https://doi.org/10.1175/1520-0493(1980)108<1212:AAMOTW>2.0.CO;2

20. Homma, T., Saltelli, A.: Importance measures in global sensitivity analysis of nonlinear models. Reliab. Eng. and Syst. Saf. **52**(1), 1–17 (1996). https://doi.org/10.1016/0951-8320(96)00002-6. http://www.sciencedirect.com/science/article/pii/0951832096000026

21. Houze, R.A.: Cloud Dynamics. International Geophysics. Elsevier Science. https://books.google.fr/books?id=5DKWGZwBBEYC (1994)

22. Irish, J.L., Resio, D.T., Cialone, M.A.: A surge response function approach to coastal hazard assessment. Part 2: quantification of spatial attributes of response functions. Nat. Hazards **51**(1), 183–205 (2009). https://doi.org/10.1007/s11069-009-9381-4

23. Iskandarani, M., Wang, S., Srinivasan, A., Thacker., W.C., Winokur, J., Knio, O.: An overview of uncertainty quantification techniques with application to oceanic and oil-spill simulations. J. Geophys. Res.: Oceans **121**(4), 2789–2808 (2016). https://doi.org/10.1002/2015JC011366

24. Jia, G., Taflanidis, A.A., Nadal-Caraballo, N.C., Melby, J.A., Kennedy, A.B., Smith, J.M.: Surrogate modeling for peak or time-dependent storm surge prediction over an extended coastal region using an existing database of synthetic storms. Nat. Hazards **81**(2), 909–938 (2016). https://doi.org/10.1007/s11069-015-2111-1

25. Kennedy, A.B.: Coauthors: origin of the hurricane Ike forerunner surge. Geophys. Res. Lett. **38**(L08608). https://doi.org/10.1029/2011GL047090. https://agupubs.onlinelibrary.wiley.com/doi/abs/10.1029/2011GL047090 (2011)

26. Köppel, M., Franzelin, F., Kröker, I., Oladyshkin, S., Santin, G., Wittwar, D., Barth, A., Haasdonk, B., Nowak, W., Pflüger, D., Rohde, C.: Comparison of data-driven uncertainty quantification methods for a carbon dioxide storage benchmark scenario. Comput. Geosci. **23**(2), 339–354 (2019). https://doi.org/10.1007/s10596-018-9785-x

27. Le Maître, O.P., Knio, O.M.: Spectral Methods for Uncertainty Quantification. Scientific Computation, Springer (2010)

28. Li, G., Curcic, M., Iskandarani, M., Chen, S.S., Knio, O.M.: Uncertainty propagation in coupled Atmosphere–Wave–Ocean prediction system: a study of hurricane Earl. Mon. Weather Rev. **147**(1), 221–245 (2019). https://doi.org/10.1175/MWR-D-17-0371.1

29. Li, G., Iskandarani, M., Le Hénaff, M., Winokur, J., Le Maître, O.P., Knio, O.M.: Quantifying initial and wind forcing uncertainties in the Gulf of Mexico. Comput. Geosci. **20**(5), 1133–1153 (2016). https://doi.org/10.1007/s10596-016-9581-4

30. Lin, N., Chavas, D.: On hurricane parametric wind and applications in storm surge modeling. J. Geophys. Res.: Atmospheres **117**(D9), n/a–n/a (2012). https://doi.org/10.1029/2011JD017126. D09120

31. Lorenz, E.N.: Empirical orthogonal functions and statistical weather prediction. Scientific report / MIT. Statistical Forecasting Project. Massachusetts Institute of Technology, Department of Meteorology. https://books.google.com/books?id=2cQIogEACAAJ (1956)

32. Luettich, R.A., Westerink J.J.: Formulation and numerical implementation of the 2D/3D ADCIRC finite element model version 44.XX (2004)

33. Mayo, T., Butler, T., Dawson, C., Hoteit, I.: Data assimilation within the advanced circulation (ADCIRC) modeling framework for the estimation of Manning's friction coefficient. Ocean Model. **76**, 43–58 (2014). https://doi.org/10.1016/j.ocemod.2014.01.001. http://www.sciencedirect.com/science/article/pii/S146350031400002X

34. Mel, R., Viero, D.P., Carniello, L., Defina, A., D'Alpaos, L.: Simplified methods for real-time prediction of storm surge uncertainty: The city of Venice case study. Adv. Water. Resour. **71**, 177–185 (2014). https://doi.org/10.1016/j.advwatres.2014.06.014. http://www.sciencedirect.com/science/article/pii/S0309170814001316

35. Molteni, F., Buizza, R., Palmer, T.N., Petroliagis, T.: The ECMWF ensemble prediction system: methodology and validation. Quart. J. Roy. Meteor. Soc. **122**(529), 73–119 (1996). https://doi.org/10.1002/qj.49712252905. https://rmets.onlinelibrary.wiley.com/doi/abs/10.1002/qj.49712252905

36. Morokoff, W.J., Caflisch, R.E.: Quasi-Monte Carlo integration. J. Comput. Phys. **122**(2), 218–230 (1995). https://doi.org/10.1006/jcph.1995.1209. http://www.sciencedirect.com/science/article/pii/S0021999185712090

37. Myers, V.A.: Storm tide frequencies on the South Carolina Coast. Tech. Rep. NWS. 16 NOAA (1975)

38. Navarro, M., Le Maître, O., Hoteit, I., George, D., Mandli, K., Knio, O.: Surrogate-based parameter inference in debris flow model. Comput. Geosci. **22**(6), 1447–1463 (2018). https://doi.org/10.1007/s10596-018-9765-1

39. NOAA/NHC: Tropical cyclone report, hurricane Gustav (AL072008). [Available online at http://ftp.nhc.noaa.gov/atcf/archive/2008/bal072008.dat.gz] (2008)

40. Powell, M.D.: Drag coefficient distribution and wind speed dependence in tropical cyclones. Final report to the NOAA joint hurricane testbed (JHT) program, 26p NOAA/atlantic oceanographic and meteorological laboratory (2006)

41. Resio, D.T., Powell, N.J., Cialone, M.A., Das, H.S., Westerink, J.J.: Quantifying impacts of forecast uncertainties on predicted storm surges. Nat. Hazards **88**(3), 1423–1449 (2017).

42. Rohmer, J., Lecacheux, S., Pedreros, R., Quetelard, H., Bonnardot, F., Idier, D.: Dynamic parameter sensitivity in numerical modelling of cyclone-induced waves: a multi-look approach using advanced meta-modelling techniques. Nat. Hazards **84**(3), 1765–1792 (2016). https://doi.org/10.1007/s11069-016-2513-8

43. Sobol, I.M.: Sensitivity estimates for nonlinear mathematical models. Math. Model. Comput. Exp. **1**, 407–414 (1993)

44. Sochala, P., De Martin, F.: Surrogate combining harmonic decomposition and polynomial chaos for seismic shear waves in uncertain media. Comput. Geosci. https://doi.org/10.1007/s10596-017-9677-5 (2017)

45. Sochala, P., Le Maître, O.: Polynomial Chaos expansion for subsurface flows with uncertain soil parameters. Adv. Water. Resour. **62**, 139–154 (2013). https://doi.org/10.1016/j.advwatres.2013.10.003. https://hal.archives-ouvertes.fr/hal-00931639

46. Song, Y.K., Irish, J.L., Udoh, I.E.: Regional attributes of hurricane surge response functions for hazard assessment. Nat. Hazards **64**(2), 1475–1490 (2012). https://doi.org/10.1007/s11069-012-0309-z

47. Taylor, G.I.: Skin friction of the wind on the earth's surface. Proc. Roy. Soc. London **A92**(637), 196–199 (1916). https://doi.org/10.1098/rspa.1916.0005. http://rspa.royalsocietypublishing.org/content/92/637/196

48. Taylor, N.R., Irish, J.L., Udoh, I.E., Bilskie, M.V., Hagen, S.C.: Development and uncertainty quantification of hurricane surge response functions for hazard assessment in coastal bays. Nat. Hazards **77**(2), 1103–1123 (2015). https://doi.org/10.1007/s11069-015-1646-5

49. Thompson, E.F., Cardone, V.J.: Practical modeling of hurricane surface wind fields. J. Waterw. Port. Coast. **122**(4), 195–205 (1996). https://doi.org/10.1061/(ASCE)0733-950X(1996)122:4(195). http://ascelibrary.org/doi/abs/10.1061/1996

50. Toro, G.R., Resio, D.T., Divoky, D., Niedoroda, A.W., Reed, C.: Efficient joint-probability methods for hurricane surge frequency analysis. Ocean Eng. **37**(1), 125–134 (2010). https://doi.org/10.1016/j.oceaneng.2009.09.004. http://www.sciencedirect.com/science/article/pii/S0029801809002236

51. Zheng, F., Westra, S., Leonard, M., Sisson, S.A.: Modeling dependence between extreme rainfall and storm surge to estimate coastal flooding risk. Water Resour. Res. **50**(3), 2050–2071 (2014). https://doi.org/10.1002/2013WR014616. https://agupubs.onlinelibrary.wiley.com/doi/abs/10.1002/2013WR014616